Performance of U/P Finite Elements Subjected To
Nearly Incompressible Linear Axisymmetric Orthotropic Conditions
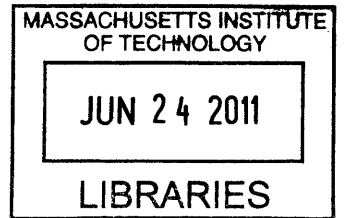
By

Robert D. Bateman

Submitted to the department of Civil and Environmental Engineering
in Partial Fulfillment of the requirements for the degree of

Master of Engineering

In Civil and Environmental Engineering
at the
Massachusetts Institute of Technology, MIT

June 2011

Signature of Author_____
Department of Civil and Environmental Engineering
May 6, 2011

Certified by_____
Jerome J. Connor
Professor of Civil and Environmental Engineering
Thesis Supervisor

Accepted by_____
Heidi M. Nepf
Chair, Departmental Committee for Graduate Students

Performance of U/P Finite Elements Subjected To Nearly Incompressible Linear Axisymmetric Orthotropic Conditions

By

Robert D. Bateman

Submitted to the department of Civil and Environmental Engineering
on May 6, 2011 in Partial Fulfillment of the requirements for the degree of

Master of Engineering

In Civil and Environmental Engineering

Finite element analysis is a vastly expanding field which provides engineers a viable instrumentation to model and measure idealized constitutive stress strain relationships for various complex physical bodies. In the field of Civil Engineering, this tool has proven very useful to analyze problems that do not have a direct closed solution guided by elementary structural mechanics. Within this field, there are many choices of finite elements, and should be chosen by the engineer to best suit the given mathematical model. For structural analysis, displacement based elements are undeniably the most used in practice. However, these elements have limitations and in such cases, other elements should be used. In foundation design, it is important to accurately model soil deformations and stresses. If the ground conditions are proven to be best modeled orthotropic instead of isotropic, then a finite element analysis should be implemented. If the soil is also shown to be saturated and exhibiting an undrained condition, a finite element analysis with standard displacement based elements will produce erroneous results due to the formulation and therefore another choice of finite element must be made. The scope of this work is to graphically show the performance of U/P finite elements subjected to nearly incompressible linear axisymmetric orthotropic conditions and its superiority over standard displacement based finite elements in this situation.

Thesis Supervisor: Jerome J. Connor

Title: Professor of Civil and Environmental Engineering

ACKNOWLEDGEMENTS

graduate with no direction into an MIT graduate. The selflessness and passion that these men exhibited in helping me understand my fundamentals is unparallel to anyone else. You four have taught me not just physics and mathematics, but also how to think for myself.

Last but not least I wish to thank all my friends who have stood by me and supported my cause. There are so many and I have been truly blessed to have met every one of you.

- Robert D. Bateman, M.Eng.

TABLE OF CONTENTS

TABLE OF FIGURES

TABLE OF TABLES

9

CHAPTER 1: INTRODUCTION AND OVERVIEW

INTRODUCTION

For many mechanical, civil, and aeronautical problems, complex solid geometry subjected to boundary conditions and various loadings need to be solved. Due to the complex nature of these problems, a finite element analysis is performed. The finite element method works with a modified version of the variational (weak form) derived from the differential formulations of solid mechanics. The finite element technique will vary depending on the modeling assumptions of the problem statement. For example, most civil engineering applications involve a linear isotropic analysis with small strains and displacements. As is the case, there are different types of finite elements that are designed to be used in different scenarios. One common problem involves a linear isotropic material which is nearly incompressible. It has been shown that for these situations a mixed U/P element is most suitable. The convergence rate is tolerable and performs much better than standard 2D 4-U node and 2D 9-U node displacement based elements. However, if the nearly incompressible continuum is modeled as orthotropic instead of isotropic, the above statement continues to hold as well. This text attempts to show this.

This thesis is to analyze the performance of U/P elements subjected to nearly incompressible linear axisymmetric orthotropic conditions. An axisymmetric case is chosen because of practical reasons. In the modeling of a large continuum body such as soil beneath a building foundation, the used of 3D finite elements can prove to be vastly expensive computationally. In such cases of modeling large unbounded arenas, 2D axisymmetric formulations are a much more efficient and cost saving modeling technique which will produce the same effect.

In order to show the effectiveness of U/P finite elements in this scenario, a literature review of this behavior must first be made (as should be the case in any finite element analysis). The following chapters which constitute this review are:

2. **Mechanical Behavior**
3. **Finite Element Analysis Formulation**

Chapter 2 discusses the mechanical behavior from which the finite element formulation is derived. A discussion will briefly show the differences between isotropic and orthotropic behavior. These conditions differ in modeling nearly incompressible conditions and a comparison of the two limitations will be shown. Next, a review of structural mechanics involving modeling axisymmetric conditions will be presented. Since the topic of this thesis involves modeling nearly incompressible orthotropic media, a good comparison is made in the modeling of soil media for foundation design. As such, this chapter concludes with a summary on analytically modeling stress in soil under a foundation load, its limitations, and why the use of a finite element analysis would prove useful in such a scenario (Coduto).

Chapter 3 provides a summary of the standard finite element formulation modeled from continuum mechanics. In this chapter, the formulation of displacement based U elements and mixed displacement pressure based U/P elements will be presented and compared. For this project, 4-U, 9-U, 4/1-U/P, and 9/3-U/P elements will be compared. Therefore, this chapter will provide on an introductory explanation of all four of these elements. For these elements to be properly judged for their expense and adequacy in the solution process, these elements shall be compared based on their strain energy convergence rates. Strain energy provides the engineer a scalar basis on which to judge element performance. As such, this chapter concludes with an introduction to modeling convergence of these various finite elements and its limitations.

4 Convergence Experiment

Chapter 4 will discuss the modeling considerations used in this experiment. An in depth comparison analysis will be made of a nearly incompressible hollow sphere using various finite elements. The hierarchical modeling philosophy will be presented to show the consequences in transitioning from modeling a physical continuum body to approximating its behavior with a finite element mathematical model. This chapter will also explain the modeling transition of modeling expensive 3D unbounded continua with an axisymmetric approximation. 2D axisymmetric modeling is an inexpensive strategy in the modeling of soil for foundation design.

This experiment will run 20 different combinations of orthotropic Poisson ratios acting on the model sphere. One material will be purely compressible, and one will act as isotropic and nearly incompressible for comparison. The 18 other combinations are a variety of nearly incompressible and compressible orthotropic materials. The results will graphically show that U/P based elements perform just as well in orthotropic conditions as in isotropic conditions for nearly incompressible material problems by means of convergence of strain energy.
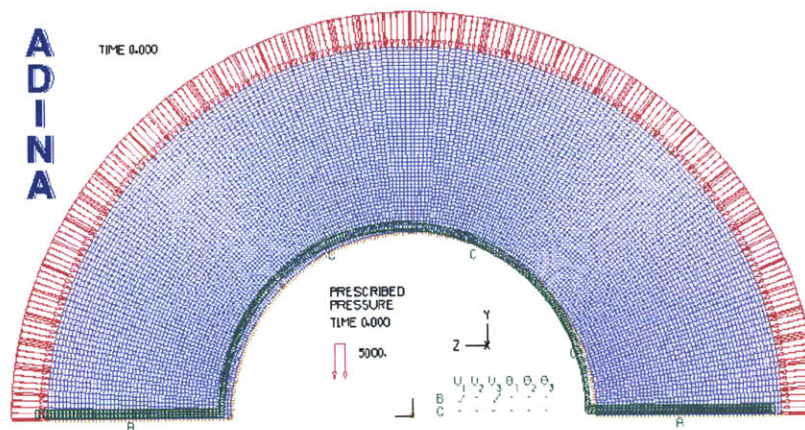
Figure 1: Axisymmetric Representation
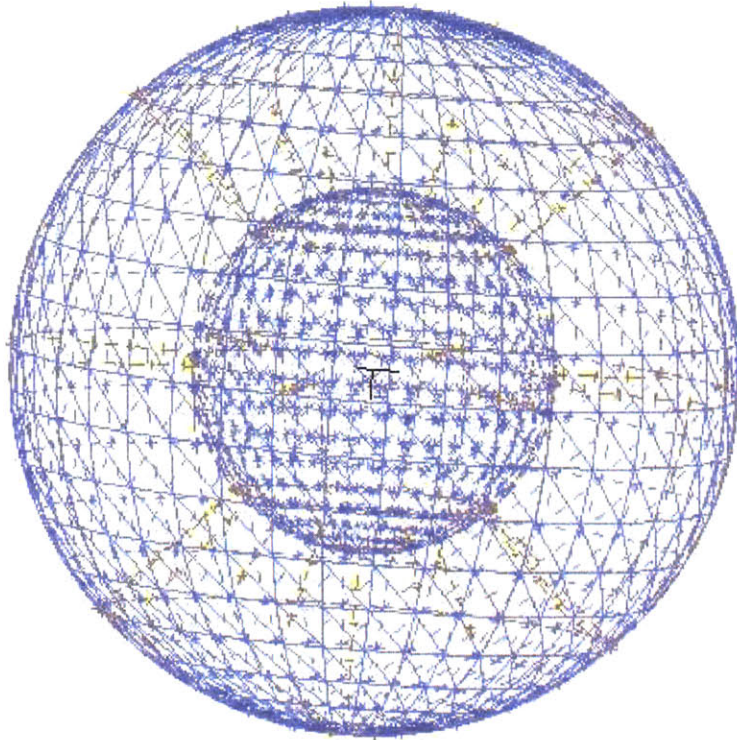
Figure 2: Experimental Model

To analyze the performance of U/P elements subjected to nearly incompressible orthotropic conditions, a comparison study of U/P elements with standard 2D 4-U node and 2D 9-U node elements will be made. For each element, the strain energy used in each FEA will be calculated using different mesh sizes and using different values of Poisson ratios. The three orthogonal modulus of elasticity parameters E_A, E_B, and E_C will all be equivalent to some fixed value. Thus, this analysis will only represent effects of changes of Poisson ratios. With these strain energy values, the linear convergence rate may be calculated as a scalar measurement of performance efficiency. The best element will have the largest linear convergence rate. Using symmetry techniques, the solid model used in this experiment shall be an axisymmetric revolution about the Z axis that emulates the hollowed sphere. The graphic of the 3D sphere subjected to uniform loading and the axisymmetric 2D representation are shown in figures 2 and 1 respectively.

14

CHAPTER 2: MECHANICAL BEHAVIOR
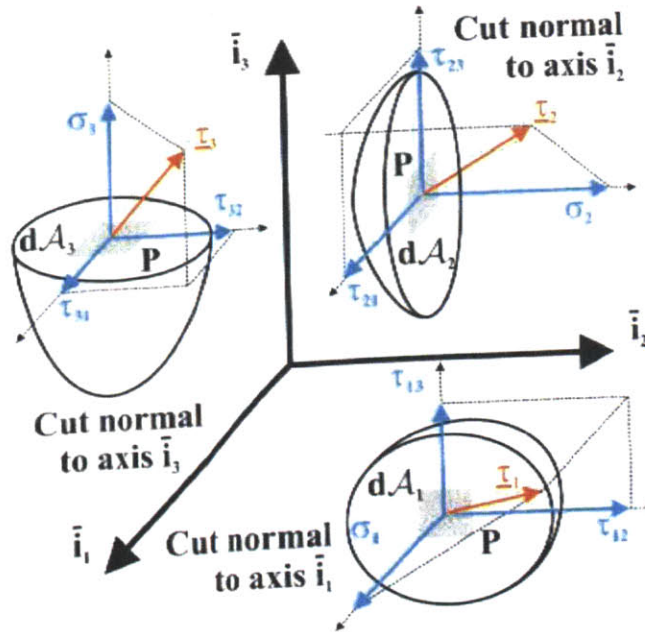
Figure 3: Global Cartesian normal and shear cauchy stresses

Chapter 2 discusses the mechanical behavior from which the finite element formulation is derived. A discussion will briefly show the differences between isotropic and orthotropic behavior. These conditions differ in modeling nearly incompressible conditions and a comparison of the two limitations will be shown. Next, a review of structural mechanics involving modeling axisymmetric conditions will be presented. Since the topic of this thesis involves modeling nearly incompressible orthotropic media, a good comparison is made in the modeling of soil media for foundation design. As such, this chapter concludes with a summary on analytically modeling stress in soil under a foundation load, its limitations, and why the use of a finite element analysis would prove useful in such a scenario. This section will explain the importance of axisymmetric modeling and how to apply this technique to modeling soil under a foundation load. Figure 3 was extracted from (Bauchau).

ISOTROPIC BEHAVIOR

An isotropic material is such that the stress strain relationship is independent of direction. Structural materials like steel provide a good example of this phenomenon. The Young's modulus and Poisson ratios are equal in all directions. Thus, the isotropic constitutive relations between stress and strain are shown (Ugural).

$$\varepsilon_x = +\frac{1}{E}\sigma_x - \frac{\nu}{E}\sigma_y - \frac{\nu}{E}\sigma_z - \alpha_x T \quad \gamma_{xy} = \frac{\tau_{xy}}{G}$$

$$\varepsilon_y = +\frac{\nu}{E}\sigma_x - \frac{1}{E_y}\sigma_y - \frac{\nu}{E}\sigma_z - \alpha_y T \quad \gamma_{yz} = \frac{\tau_{yz}}{G}$$

$$\varepsilon_z = +\frac{\nu}{E}\sigma_x - \frac{\nu}{E}\sigma_y - \frac{1}{E}\sigma_z - \alpha_z T \quad \gamma_{zx} = \frac{\tau_{zx}}{G}$$

ORTHOTROPIC BEHAVIOR

An orthotropic material is such that the stress strain relationship is not independent of direction. In particular, for a given Cartesian axis, the Young's modulus and Poisson ratio values in a given direction do not match the values given in the other two orthogonal directions. Hence the orthotropic relations of stress and strain can be generalized in the following form. Materials such as timber or composite reinforced concrete behave in manner. Figure 4 illustrates the orthotropic behavior of wood due to the differences in grain in each of the main orthogonal directions (Breyer).

Maxwell's Reciprocal Theorem states that the constitutive matrix is symmetric. Thus

$$\frac{E_x}{\nu_{xy}} = \frac{E_y}{\nu_{yx}} \quad \frac{E_y}{\nu_{yz}} = \frac{E_z}{\nu_{zy}} \quad \frac{E_z}{\nu_{zx}} = \frac{E_x}{\nu_{xz}}$$

16
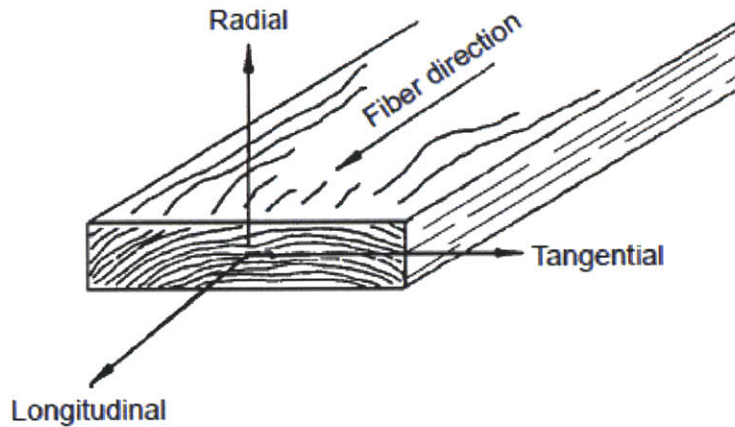
Figure 4: Orthotropic Directions of Timber

$$\varepsilon_x = +\frac{1}{E_x}\sigma_x - \frac{v_{yx}}{E_y}\sigma_y - \frac{v_{zx}}{E_z}\sigma_z - \alpha_x T \qquad \gamma_{xy} = \frac{\tau_{xy}}{G_{xy}}$$

$$\varepsilon_y = +\frac{v_{xy}}{E_x}\sigma_x - \frac{1}{E_y}\sigma_y - \frac{v_{zy}}{E_z}\sigma_z - \alpha_y T \qquad \gamma_{yz} = \frac{\tau_{yz}}{G_{yz}}$$

$$\varepsilon_z = +\frac{v_{xz}}{E_x}\sigma_x - \frac{v_{yz}}{E_y}\sigma_y - \frac{1}{E_z}\sigma_z - \alpha_z T \qquad \gamma_{zx} = \frac{\tau_{zx}}{G_{zx}}$$

With these conditions, it is also noted that there is more than one shear modulus G.

INCOMPRESSIBLE MEDIA CONDITIONS

A material is said to be incompressible if the volume under traction loading remains constant. The geometry may move but the volume in the final configuration must equal the volume of the original configuration. In elementary mechanics, this is also expressed that the dilatation of the material must equal to zero.

$$e = \varepsilon_x + \varepsilon_y + \varepsilon_z = -\frac{p}{k} = 0$$

17

The variables p and k are labeled the hydrostatic pressure and bulk modulus respectively. For incompressible conditions, k becomes infinite because hydrostatic pressure is not zero. These values are intimately related to Poisson's ratio for both isotropic and orthotropic cases. In the development of a structural mathematical model, the condition of incompressibility fails if the constitutive relation is chosen as either plane strain or axisymmetric. However, the formulation of the plane stress law remains unaffected.

$$C_{axisymmetric} = \frac{E(1-2v)}{(1+v)(1-2v)} \begin{pmatrix} 1 & \frac{v}{1-v} & 0 & \frac{v}{1-v} \\ \frac{v}{1-v} & 1 & 0 & \frac{v}{1-v} \\ 0 & 0 & \frac{1-2v}{2(1-v)} & 0 \\ \frac{v}{1-v} & \frac{v}{1-v} & 0 & 1 \end{pmatrix}$$

In the case of an isotropic material for either axisymmetric or plane strain, there is a restriction on the value of Poisson's ratio as shown above. If $v = 0.5$, the material is incompressible. The constitutive matrix C is divided by 0 and the matrix reaches infinite values. Because the stiffness matrix K relies on the constitutive matrix C, K will also approach infinity. Figure 5 illustrates isotropic incompressible media subjected to loading (Coduto). The original volume is conserved.
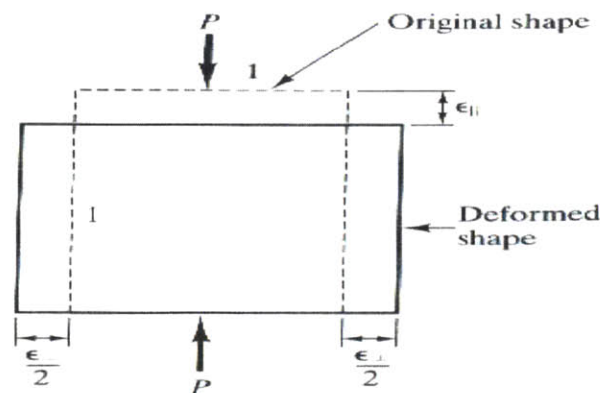
Figure 5: Isotropic Incompressible Media

For orthotropic behavior, a one to one correspondence must exist between stress and strain (linear analysis guarantees a unique solution). Therefore the determinant of the constitutive matrix C must be invertible and thus have a determinant not equal to zero (Ting). Mathematically, this requires the first and second block determinants to be positive. As consequence, the following restrictions are presented (Lempriere).

$$f(E_A E_B E_C G_A G_B G_C) > 0$$

$$v_{AB} v_{BC} v_{CA} < 0.5 \left(1 - v_{AB}^2 \frac{E_A}{E_B} - v_{BC}^2 \frac{E_B}{E_C} - v_{CA}^2 \frac{E_C}{E_A}\right) \leq 0.5$$

$$|v_{i,j}| < \sqrt{\frac{E_j}{E_i}} \quad i,j = A,B,C$$

If the Poisson ratios are chosen such that the above restrictions are not satisfied, the orthotropic material will be classified as incompressible and a solution will not be obtained.

For nearly incompressible solutions:

$$v_{AB} v_{BC} v_{CA} < 0.49999 \left(1 - v_{AB}^2 \frac{E_A}{E_B} - v_{BC}^2 \frac{E_B}{E_C} - v_{CA}^2 \frac{E_C}{E_A}\right) = 0.49999$$

AXISYMMETRIC MODELING

In structural analysis, modeling the constitutive relations for a given 3D physical body can be rather difficult. Axisymmetric modeling is a 2D scheme that provides an efficient method to easily model 3D problems that are symmetric in a revolution about some defined axis. Figure 6 illustrates this behavior (Bucalem).The equilibrium equations of stress are transformed from a Cartesian to a cylindrical coordinate system and are as follows:

$$\frac{\partial \tau_{rr}}{\partial r} + \frac{1}{r}\frac{\partial \tau_{r\theta}}{\partial \theta} + \frac{\partial \tau_{rz}}{\partial z} + \frac{\tau_{rr} - \tau_{\theta\theta}}{r} + f_r^B = 0$$

$$\frac{\partial \tau_{\theta r}}{\partial r} + \frac{1}{r}\frac{\partial \tau_{\theta\theta}}{\partial \theta} + \frac{\partial \tau_{\theta z}}{\partial z} + 2\frac{\tau_{\theta r}}{r} + f_\theta^B = 0$$

$$\frac{\partial \tau_{zr}}{\partial r} + \frac{1}{r}\frac{\partial \tau_{z\theta}}{\partial \theta} + \frac{\partial \tau_{zz}}{\partial z} + \frac{\tau_{zr}}{r} + f_z^B = 0$$
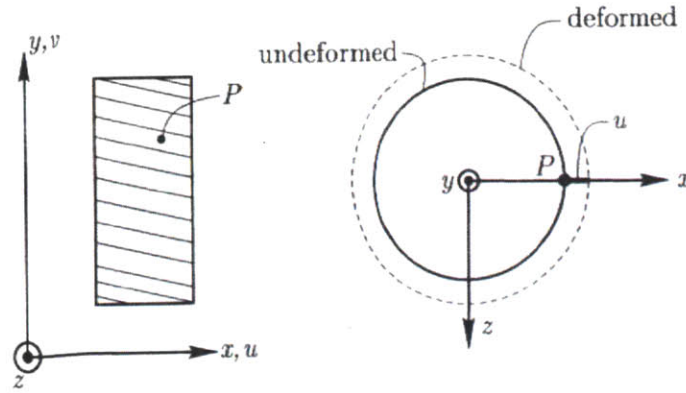
Figure 6: Axisymmetric 2D element representation of a cylinder

For an axisymmetric case about the z axis, the following restrictions are made:

$$[f_\theta^B = 0] \quad \left[\frac{\partial}{\partial \theta} = 0\right] \quad [\tau_{r\theta} = \tau_{z\theta} = 0]$$

$$\left(\frac{\partial \tau_{rr}}{\partial r} + \frac{\partial \tau_{rz}}{\partial z} + \frac{\tau_{rr} - \tau_{\theta\theta}}{r} + f_r^B = 0\right) \quad \left(\frac{\partial \tau_{zr}}{\partial r} + \frac{\partial \tau_{zz}}{\partial z} + \frac{\tau_{zr}}{r} + f_z^B = 0\right)$$

The above formulas are the axisymmetric force equilibrium equations. In practice, to implement these equations a 2D shape that represents the solid formed if revolved around a given axis is chosen. If that axis is labeled z, then the 2D shape is in a Cartesian xy plane. Therefore, the above axisymmetric equation may be rewritten as:

$$\left(\frac{\partial \tau_{xx}}{\partial x} + \frac{\partial \tau_{xy}}{\partial y} + \frac{\tau_{xx} - \tau_{zz}}{x} + f_x^B = 0\right) \quad \left(\frac{\partial \tau_{xy}}{\partial x} + \frac{\partial \tau_{yy}}{\partial y} + \frac{\tau_{xy}}{x} + f_y^B = 0\right)$$

20

This chapter concludes with a brief exploration of geotechnical analysis in foundation design. When a structure is built, it must have an adequate foundation to create an effective load path that allows the structural load to be safely transmitted to the soil below. The transmission must be such that the soil does not fail beneath the building. Failure of soil is defined in terms of slippage of the soil particles or excessive deformations. In 1885, mathematician Joseph Boussinesq formulated a set of equations that allow adequate modeling of induced soil stresses from a point load by modeling the soil as an isotropic infinite half space. Figure 7 illustrates the implementation of these formulas (Coduto).
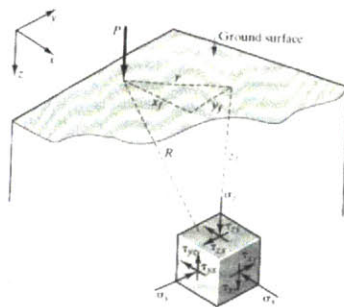
Figure 7: Boussinesq Infinite Half Space Modeling
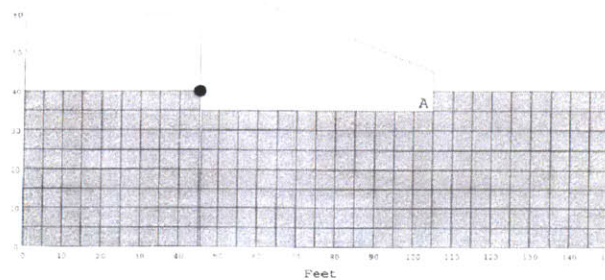
Figure 8: Finite element modeling of soil under foundation

$$R = \sqrt{x^2 + y^2 + z^2} \qquad r = \sqrt{x^2 + y^2}$$

$$\sigma_x = \frac{P}{2\pi}\left[\frac{3x^2 z}{R^5} - (1-2v)\left(\frac{x^2 - y^2}{Rr^2(R+z)} + \frac{y^2 z}{R^3 r^2}\right)\right] \qquad \sigma_y = \frac{P}{2\pi}\left[\frac{3y^2 z}{R^5} - (1-2v)\left(\frac{y^2 - x^2}{Rr^2(R+z)} + \frac{x^2 z}{R^3 r^2}\right)\right]$$

$$\tau_{xy} = -\tau_{xy} = \frac{P}{2\pi}\left[\frac{3xyz}{R^5} - (1-2v)\left(\frac{(2R+2)xy}{(R+z^2)R^3}\right)\right] \qquad R = \sqrt{x^2 + y^2 + z^2} \qquad r = \sqrt{x^2 + y^2}$$

Shown above are the equations for the lateral normal and shear stresses of a soil subjected to a point load P. Lateral stresses are mainly important in retaining wall design because these are the stresses that are applied horizontally on the wall considered. The variables x,y,z are the

displacements from the stress point to the applied point load P. The variable z is always positive. It is noticed that the lateral normal and shear stresses rely on Poisson's ratio. For an isotropic analysis, values of Poisson's ratio for various soils and rocks have been tabulated in table 1 and have proven to be sufficiently precise in foundation design (Coduto).

Soil Media and Poisson's Ratio Ranges			
Saturated Soil, Undrained	0.50	Loose Sand, Drained	$0.10-0.30$
Partially Saturated Clay	$0.30 = 0.40$	Sandstone	$0.25-0.30$
Dense Sand, Drained	$0.30-0.40$	Granite	$0.23-0.27$

Table 1: Isotropic Poisson's ratio range for various soil media

Thus, if the soil is conditioned to be modeled as orthotropic, these equations may not be used. If the loading cannot be approximated by a point load (as is the general case) numerical methods must be used such as charted approximation solutions or a finite element analysis. In a 2D finite element analysis (common), a plane strain model would be sufficient. For 3D modeling, it is efficient to model using axisymmetric 2D elements to conserve computational expense. Because soil mechanics analyzes this media as an infinite halfspace, the energy provided by these elements need to be released and modeled with infinite boundaries (Kim). It is suggested by Cook that infinite elements be used. Figures 8 and 9 depict this FEA modeling (Cook).
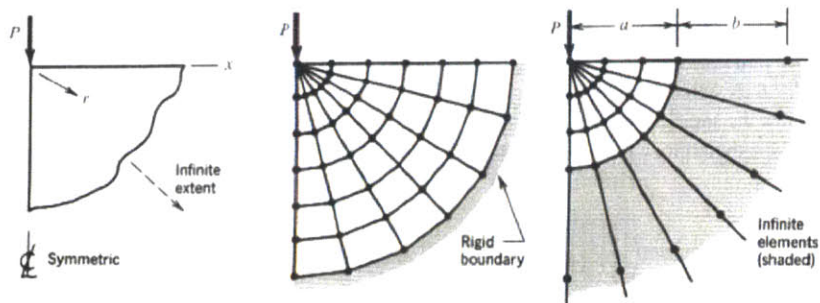
Figure 9: Load P on an axisymmetric body of infinite extent

22

CHAPTER 3: FINITE ELEMENT ANALYSIS FORMULATION
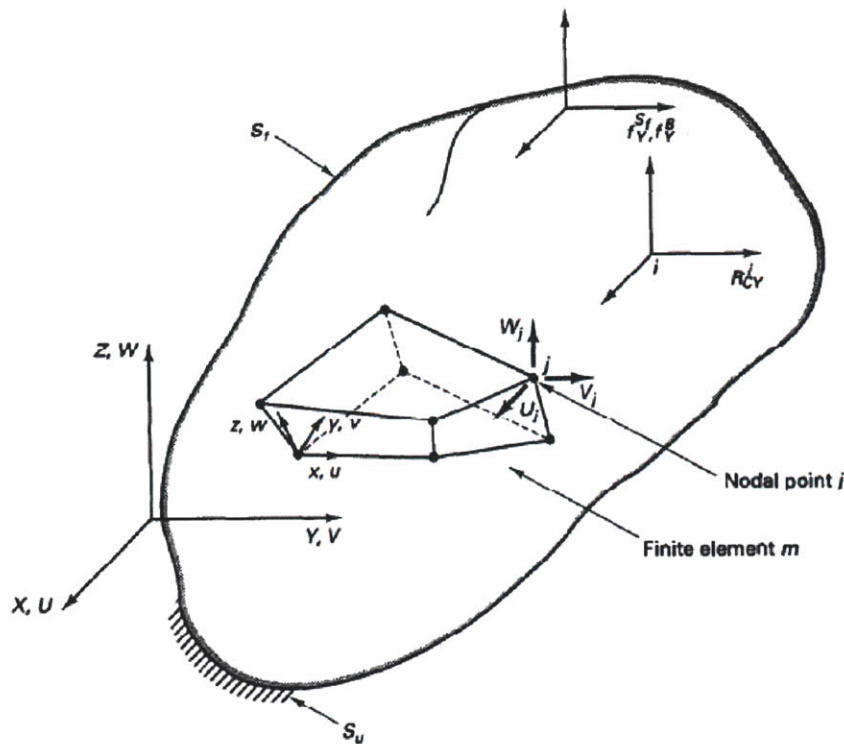
Figure 10: Finite element representation of a solid continuum physical body

Before a finite element analysis can begin, it is important to understand the formulation of a finite element analysis and the calculations computed in its results. In this section, a quick review of the displacement based element formulation of the finite element method is presented. Then, the mixed displacement pressure formulation will be presented and comparisons will be made to the original displacement method. Then a quick comparison in known facts between two dimensional 4-U node, 9-U Node, 4/1-U/P and 9/3-U/P elements will be tabulated. Lastly, a primer of calculations considered in the evaluation of strain energy for a displacement based solution is shown and the convergence qualitative effects for displacement pressure elements. Figure 10 was extracted from (Bathe).

In solid mechanics, every continuum mathematical model is governed by a set of differential equations, known as the differential formulation, which relates the behavior of the displacements and strains the body is experiencing to the stresses and traction forces acted upon itself. The term "continuum mathematical model" is used because any solution governed by solid mechanics has some error and should only be reflected as a model that best approximates the real behavior with tolerable limits. For simplistic mathematical models (uniaxial bar in tension for example), the solution of the differential formulation is widely known and has a closed form solution. However, as the complexity of the model increases, closed form solutions may not be possible by hand calculation or even with aid of a computer. This presents a problem for many applications such as modeling soil in foundation design. Thus, either an empirical formulation must be made that relates test data to a best fitting curve (this can be very expensive) or a finite element analysis may be implemented to provide a computational approximation to the continuum mathematical model.

PRINCIPLE OF VIRTUAL WORK OF A CONTINUUM SOLID BODY

To utilize a finite element formulation, the variational formulation (weak form) of the continuum mathematical model must be stated. The following is a derivation the variational form from the differential formulation (Bathe). The derivation of this formulation from the differential formulation is displayed in Appendix A: Principle of Virtual Displacements Derivation.

$$\int_V \tau_{ij} \bar{\varepsilon}_{ij} dV = \int_V f_i^B \bar{U}_i dV + \int_{S_f} f_i^{S_f} \bar{U}_i^{S_f} dS_f$$

As will be shown, this equation provides the basis for utilizing displacement based finite elements. The key is to approximate the above integral equation as a summation.

CONSTITUTIVE RELATIONS OF ORTHOTROPIC BEHAVIOR

In solid mechanics, there is a relationship between the internal and external forces on the solid body, and the strains within the body. This relationship is known as the constitutive relationship and is dependent on the choice of mathematical model used. In chapter two, the constitutive law for axisymmetric behavior of a solid continuum has been presented along with a summary of its limitations due to incompressible isotropic and orthotropic behavior respectively. The following provides additional information for the effects of orthotropic behavior for axisymmetric finite element modeling.

ORTHOTROPIC BEHAVIOR FOR AXISYMMETRIC FINITE ELEMENT MODELING

In a finite element formulation, the constitutive matrix relations for a mathematical continuum model are unmodified in the finite element analysis. The following legend and figure 11 illustrates the local coordinate system for modeling orthotropic behavior in a finite element (Adina).

The directions A,B,C are defined below:

A = direction of element

B = orthogonal to A but within plane of solid

C = orthogonal to both A and B, out of plane
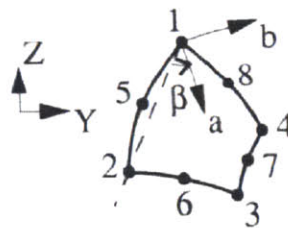
Figure 11: Orthotropic local coordinate system

Each element composing the finite element mesh contains its own local coordinate system ABC. A transformation matrix is used to relate this mapping to the global Cartesian XYZ system. The plane stress and plane strain matrix representations of orthotropic linear behavior is:

(Plane Stress)

$$
\begin{pmatrix} \varepsilon_{AA} \\ \varepsilon_{BB} \\ \varepsilon_{CC} \\ \varepsilon_{AB} \end{pmatrix} =
\begin{pmatrix}
\dfrac{1}{E_A} & -\dfrac{V_{AB}}{E_B} & -\dfrac{V_{AC}}{E_C} & 0 \\[8pt]
-\dfrac{V_{BA}}{E_A} & \dfrac{1}{E_B} & -\dfrac{V_{BC}}{E_C} & 0 \\[8pt]
-\dfrac{V_{CA}}{E_A} & -\dfrac{V_{CB}}{E_B} & \dfrac{1}{E_C} & 0 \\[8pt]
0 & 0 & 0 & \dfrac{1}{G_{AB}}
\end{pmatrix}
\begin{pmatrix} \sigma_A \\ \sigma_B \\ \sigma_C = 0 \\ \sigma_{AB} \end{pmatrix}
$$

(Plane Strain)

$$
\begin{pmatrix} \varepsilon_{AA} \\ \varepsilon_{BB} \\ \varepsilon_{CC} = 0 \\ \varepsilon_{AB} \end{pmatrix} =
\begin{pmatrix}
\dfrac{1}{E_A} & -\dfrac{V_{AB}}{E_B} & -\dfrac{V_{AC}}{E_C} & 0 \\[8pt]
-\dfrac{V_{BA}}{E_A} & \dfrac{1}{E_B} & -\dfrac{V_{BC}}{E_C} & 0 \\[8pt]
-\dfrac{V_{CA}}{E_A} & -\dfrac{V_{CB}}{E_B} & \dfrac{1}{E_C} & 0 \\[8pt]
0 & 0 & 0 & \dfrac{1}{G_{AB}}
\end{pmatrix}
\begin{pmatrix} \sigma_A \\ \sigma_B \\ \sigma_C \\ \sigma_{AB} \end{pmatrix}
$$

(Axisymmetric)

$$
\begin{pmatrix} \varepsilon_{AA} \\ \varepsilon_{BB} \\ \varepsilon_{CC} = 0 \\ \varepsilon_{AB} \end{pmatrix} =
\begin{pmatrix}
\dfrac{1}{E_A} & -\dfrac{V_{AB}}{E_B} & -\dfrac{V_{AC}}{E_C} & 0 \\[8pt]
-\dfrac{V_{BA}}{E_A} & \dfrac{1}{E_B} & -\dfrac{V_{BC}}{E_C} & 0 \\[8pt]
-\dfrac{V_{CA}}{E_A} & -\dfrac{V_{CB}}{E_B} & \dfrac{1}{E_C} & 0 \\[8pt]
0 & 0 & 0 & \dfrac{1}{G_{AB}}
\end{pmatrix}
\begin{pmatrix} \sigma_A \\ \sigma_B \\ \sigma_C \\ \sigma_{AB} \end{pmatrix}
$$

The displacement based finite element mesh will yield an unsatisfactory solution. For this project, the boundaries of this restriction are tested for different Poisson ratios. Using the

strain energy formulation as described above, a mapping will be made to show how convergence is affected as models approach incompressible conditions. Lastly, it will be shown how U/P hybrid elements handle convergence performance and to prove that U/P elements are the preferred element to utilize in orthotropic linear analysis just as they were for isotropic nearly incompressible materials.

DISPLACEMENT BASED FINITE ELEMENT DISCRETIZATION OF THE VARIATIONAL FORM

DIPLACEMENT INTERPOLATION FIELDS

The variational formulation of a solid continuum body is elegant but it does not provide much use in a solution to the mathematical model (A differential equation is "easier" to solve than an integral equation") (Bathe). The utilization of the variational formulation becomes apparent when the finite element method is implemented. For a complex continuum model, the problem becomes difficult because the relationship between traction and displacement is unknown. At best, an approximation (interpolation) must be made.

The finite element method approaches this by discretizing the continuum into finite elements. These elements are material, bounded by a nodal configuration and connected via these nodes. Forces are applied to these finite elements and deformations are created. The interpolation assumption is that the displacement field within a finite element may be completely described if the nodal point displacements are known. Thus for a given finite element:

$$\mathbf{u}^{(m)}(x, y, z) = \mathbf{H}^{(m)}(x, y, z)\hat{\mathbf{U}}$$

$$\hat{\mathbf{U}}^T = [\mathbf{U_1}^T \quad \mathbf{U_2}^T \quad \dots \quad \mathbf{U_i}^T \quad \dots \quad \mathbf{U_N}^T]$$

$$\mathbf{U_i}^T = [u_i \quad v_i \quad w_i] = \text{displacement vector for node i}$$

The displacement vector at any (x,y,z) point in the element $\mathbf{u}^{(m)}(x, y, z)$, is defined by the nodal displacements $\hat{\mathbf{U}}$ and an interpolation matrix $\mathbf{H}^{(m)}(x, y, z)$. To be valid, the equation must hold true for the nodal displacements themselves. Thus if (x, y, z) is chosen to be the location of a node, $\mathbf{H}^{(m)}(x, y, z)$ but be such that $\mathbf{u}^{(m)}(x, y, z)$ = the node's displacement.

DISCRETIZATION OF PVW EQUATION

As discussed above, the displacements of any point within an element is completely defined by the nodal points (Bathe):

$$\mathbf{u}^{(m)}(x, y, z) = \mathbf{H}^{(m)}(x, y, z)\hat{\mathbf{U}}$$

$$\mathbf{\varepsilon}^{(m)}(x, y, z) = \mathbf{B}^{(m)}(x, y, z)\hat{\mathbf{U}}$$

If the strain field of an element m is obtained, then utilizing a constitutive relationship the stress field can be obtained:

$$\mathbf{\tau}^{(m)}(x, y, z) = \mathbf{C}^{(m)}\mathbf{\varepsilon}^{(m)}(x, y, z) \quad \text{(If no intial stresses are present prior to loading)}$$

If the principle of virtual displacements holds for a continuum body, then it must also hold for a finite dizretization of the body (The volume of a body is the sum of the volumes of all pieces making the body).

Thus the principle of virtual work may be transformed to accommodate a finite element mesh.

$$\int_V \tau_{ij}\bar{\varepsilon}_{ij}dV = \int_V f_i^B \bar{U}_i dV + \int_{S_f} f_i^{S_f}\bar{U}_i^{S_f}dS_f$$

$$\sum_m \int_{V^{(m)}} \bar{\mathbf{\varepsilon}}^{(m)T}\mathbf{\tau}^{(m)}\,dV^{(m)} = \sum_m \int_{V^{(m)}} \bar{\mathbf{u}}^{(m)T}\mathbf{f}^{B(m)}dV^{(m)} + \sum_m \int_{S_f^{(m)}} \bar{\mathbf{u}}^{S_f(m)T}\mathbf{f}^{S_f(m)}dS_f^{(m)}$$

28

$$\widehat{U}^T \left\{ \sum_m \int_{V^{(m)}} B^{(m)T} C^{(m)} B^{(m)} \, dV^{(m)} \right\} \widehat{U} = \widehat{U}^T \left\{ \sum_m \int_{V^{(m)}} H^{(m)T} f^{B(m)} dV^{(m)} + \sum_m \int_{S_f^{(m)}} H^{S_f(m)T} f^{S_f(m)} dS_f^{(m)} \right\}$$

The above equation must hold for any arbitrary virtual displacement. Thus, the variational finite element formulation transforms into:

$$\left\{ \sum_m \int_{V^{(m)}} B^{(m)T} C^{(m)} B^{(m)} \, dV^{(m)} \right\} \widehat{U} = \left\{ \sum_m \int_{V^{(m)}} H^{(m)T} f^{B(m)} dV^{(m)} + \sum_m \int_{S_f^{(m)}} H^{S_f(m)T} f^{S_f(m)} dS_f^{(m)} \right\}$$

$$K\widehat{U} = R$$

$$K = \sum_m \int_{V^{(m)}} B^{(m)T} C^{(m)} B^{(m)} \, dV^{(m)}$$

$$R = \sum_m \int_{V^{(m)}} H^{(m)T} f^{B(m)} dV^{(m)} + \sum_m \int_{S_f^{(m)}} H^{S_f(m)T} f^{S_f(m)} dS_f^{(m)}$$

DISPLACEMENT PRESSURE U/P BASED FINITE ELEMENT DISCRETIZATION

The mixed displacement pressure U/P based formulation is derived in a similar fashion as the displacement based formulation but with some noticeable alterations. In the U/P formulation, hydrostatic pressure nodes have been added to the degrees of freedom and are independent of the displacement nodal points. Thus in the matrix equation, the displacement vector is now a vector of displacements and pressures.

$$K\widehat{U}_{U/P} = R_{U/P}$$

$$\widehat{U}_{U/P}^T = \begin{bmatrix} U_1^T & U_2^T & \dots & U_i^T & \dots & U_N^T & | & P_1^T & P_2^T & \dots & P_j^T & \dots & P_M^T \end{bmatrix}$$

$$R_{U/P}^T = \begin{bmatrix} R_1^T & R_2^T & \dots & R_i^T & \dots & R_N^T & | & 0_1^T & 0_2^T & \dots & 0_j^T & \dots & 0_M^T \end{bmatrix}$$

For this type of mixed formulation, there is a limitation in efficiency of the N/M ratio. If there are too many pressure nodes, the element will lock and produce undesirable results. From experience and mathematical proof, it has been shown that for 4 and 9 node displacement elements, 1 and 3 pressure nodes are the optimum respectively. Thus 4/1 and 9/3 U/P elements are used in practice.

PRESSURE INTERPOLATION FIELDS

For U/P elements, pressure interpolation fields may either share the same nodal points as the chosen nodal displacements, or may be random within the element. These interpolation fields follow the same rules as described for the displacement interpolation fields.

DISCRETIZATION OF PVW EQUATION

Just as in the displacement based formulation, the finite element discretization must satisfy the conditions of equilibrium, compatibility, and follow a chosen constitutive relationship. From the variational formulation of a continuum body we have

$$\int_V \bar{\varepsilon}^T C \varepsilon dV = R$$

From chapter 2, the dilation e, bulk modulus k, and hydrostatic pressure p of a material under small strains is described as

$$e = \varepsilon_x + \varepsilon_y + \varepsilon_z = -\frac{p}{k}$$

$$k = \frac{E}{3(1-2v)} \qquad p = -ke$$

Using these parameters, the normal and shearing stresses in the body can now be described as a summation of the hydrostatic and deviatoric stresses.

$$\tau_{ij} = -p\delta_{ij} + 2G\varepsilon'_{ij} \qquad p = -\frac{\tau_{kk}}{3} \qquad \varepsilon'_{ij} = \varepsilon_{ij} - \frac{e}{3}\delta_{ij}$$

This formulation features the kronecker delta function which signifies that only normal stresses utilize the hydrostatic term.

Inserting these definitions into the PVW equation reveals

$$\int_V \overline{\varepsilon'}^T C'\varepsilon' dV + \int_V \overline{e}^T p dV = R$$

The hydrostatic pressure term p is unknown and therefore, the formula needs an additional equation.

$$p + ke = 0$$

$$\int_V \overline{p}(p + ke)dV = 0$$

$$-\int_V \overline{p}\left(e + \frac{p}{k}\right)dV = 0$$

Thus the following equation may now be discretized in the same methodology used for the displacement based formulation. However, the p term introduces additional degrees of freedom and so the finite element assemblage formulations for a U/P element are

$$\hat{U}_{U/P}^T = \begin{bmatrix} U_1^T & U_2^T & \cdots & U_i^T & \cdots & U_N^T & | P_1^T & P_2^T & \cdots & P_j^T & \cdots & P_M^T \end{bmatrix}$$

$$u^{(m)}(x,y,z) = H^{(m)}(x,y,z)\hat{U}$$

$$p^{(m)}(x,y,z) = H_P^{(m)}(x,y,z)\hat{p}$$

$$e^{(m)}(x,y,z) = B_V^{(m)}(x,y,z)\hat{U}$$

$$\varepsilon'^{(m)}(x, y, z) = B_D^{(m)}(x, y, z)\hat{U}$$

Factoring out the virtual displacement and pressures from the formulation will result in the mixed formulation stiffness matrix which relates the nodal displacement and hydrostatic pressure degrees of freedom with the applied external forces.

$$K\hat{U}_{U/P} = R_{U/P}$$

$$\begin{bmatrix} K_{UU} & K_{UP} \\ K_{PU} & K_{PP} \end{bmatrix} \begin{bmatrix} \hat{U} \\ \hat{p} \end{bmatrix} = \begin{bmatrix} R \\ 0 \end{bmatrix}$$

$$K_{UU} = \int_V B_D^T C' B_D dV \qquad K_{UP} = -\int_V B_V^T H_P dV$$

$$K_{PU} = -\int_V H_P^T B_V dV \qquad K_{PP} = -\int_V H_P^T \frac{1}{k} H_P dV$$

The use of static condensation on the matrix formulation results in an equation for stiffness of the element regarding nodal displacements and strains. Thus the nodal displacements may be directly solved.

$$\left(K_{UU} - K_{UP}K_{PP}^{-1}K_{PU}\right)\hat{U} = R$$

Consequently, static condensation cannot be performed for an incompressible analysis because the bulk modulus k will approach an infinite value. Thus, $K_{PP} = 0$ and the above equation cannot be constructed. To mitigate this obstacle, in practice the Poisson's ratio is not taken at its limiting value (0.5 for isotropic) but to nearly incompressible conditions such as 0.499999....

Thus in practice, the U/P finite element family models incompressible behavior as nearly incompressible (Bathe). In the case of the foundation design problem, the soil for an undrained saturated soil maybe modeled as nearly incompressible.

It should be noted that this example for isotropic behavior is easily extended to orthotropic behavior except that the Poisson's ratios of the material may reach values greater than 0.5 but must stay within bounds of the limitations discussed in chapter 2.

ISOPARAMETRIC ELEMENTS

When a given body is discretized into a finite element mesh, the individual finite elements in general consist of different sizes and shapes. In order to solve the finite element equation, the stiffness contributions from each element must be calculated and summed to equate a global stiffness matrix that represents the entire body (Moaveni). The geometry of each element is different and the interpolation field of each element is different which approaching directly can be very expensive and impractical to calculate. To aid in this process, each element has its own local coordinate system. The stiffness of the element is calculated by integrating over this local coordinate system and then related by a transformation equation to the global coordinate system of the body. Furthermore, each element is related to an isoparametric square element via a transformation. This allows all stiffness calculations to be similar for each element and the solution process to approach much more quickly. The following explores this procedure.

UV SPACE TRANSFORMATION

The following is the transformation equation that allows isoparametric elements to relate x,y,z space to r,s space for a two dimensional element. Appendix B develops the proof for this transformation equation and can be found as a problem in (Larson). The following can also be used proving the transformation equation from x,y,z space to r,s,t space by using Stoke's Theorem in exchange for Green's Theorem. However, because this project involves 2D-axisymetric modeling, the 2D transformation equation will be proved.

33

$$\iint_\Omega f(x,y)\,dxdy = \iint_\Omega \frac{\partial F}{\partial x}\,dxdy = \oint_{C_1} F\,dy = \iint_\Sigma f(x(r,s),y(r,s))\frac{\partial(x,y)}{\partial(r,s)}\,drds$$

$$\frac{\partial(x,y)}{\partial(r,s)} = \begin{vmatrix} \dfrac{\partial x}{\partial r} & \dfrac{\partial x}{\partial s} \\ \dfrac{\partial y}{\partial r} & \dfrac{\partial y}{\partial s} \end{vmatrix} = \left|\left(\frac{\partial x}{\partial r}\frac{\partial y}{\partial s} - \frac{\partial y}{\partial r}\frac{\partial x}{\partial s}\right)\right| = |\det(J)|$$

The above integral states that if a change of variables is used (as is the case for isoparametric elements) then the equation must include an additional component which is the absolute determinant of the Jacobian matrix. In the case of 2D axisymmetric revolutions, two Jacobians are calculated. One for the x,y to r,s space and one from Cartesian to cylindrical coordinates. The later Jacobian is R where R is the distance from the revolution axis to the center of the isoparimetric element.

INTERPOLATION FUNCTIONS

As stated above, a complex continuum body rarely has a closed formed solution for a given loading. In the finite element formulation, the body is discretized into finite elements connected to adjacent elements by means of nodes. These nodes are where the degrees of freedom are applied (u,v for 2D and u,v,w for 3D). All points within the element are described by a function involving the nodal D.O.F's. These functions are called "interpolation functions" and essentially describe the behavior between nodes in terms of those nodes. However, to describe the behavior for finite element of arbitrary geometry and so to simplify we perform the following. Tables 2 and 3 were extracted from (Bathe).

1: Take the element of consideration and represent it in r-s space as a square (cube in 3D) with length 2 and situated at the origin.

2: Express displacement vector for the r-s representation in terms of its interpolation functions which are known.

3: Utilize the primary property of an isoparametric element that the geometry is also expressed with the same interpolation functions.

4: Compute the Jacobian relating the transformation from x-y space to r-s space

Interpolation functions for a 2D Element in r-s space

		$i = 5$	$i = 6$	$i = 7$	$i = 8$	$i = 9$
$h_1 =$	$\frac{1}{4}(1+r)(1+s)$	$-\frac{1}{2}h_9$	....		$-\frac{1}{2}h_8$	$-\frac{1}{4}h_9$
$h_2 =$	$\frac{1}{4}(1-r)(1+s)$	$-\frac{1}{2}h_9$	$-\frac{1}{2}h_9$	....		$-\frac{1}{4}h_9$
$h_3 =$	$\frac{1}{4}(1-r)(1-s)$	....	$-\frac{1}{2}h_9$	$-\frac{1}{2}h_9$	....	$-\frac{1}{4}h_9$
$h_4 =$	$\frac{1}{4}(1+r)(1-s)$	....		$-\frac{1}{2}h_9$	$-\frac{1}{2}h_8$	$-\frac{1}{4}h_9$
$h_5 =$	$\frac{1}{2}(1-r^2)(1+s)$	....				$-\frac{1}{4}h_9$
$h_6 =$	$\frac{1}{2}(1-s^2)(1-r)$	....				$-\frac{1}{4}h_9$
$h_7 =$	$\frac{1}{2}(1-r^2)(1-s)$	....				$-\frac{1}{4}h_9$
$h_8 =$	$\frac{1}{2}(1-s^2)(1+r)$	....				$-\frac{1}{4}h_9$
$h_9 =$	$\frac{1}{4}(1-r^2)(1-s^2)$	....				

Table 2: Interpolation functions for a 2D Element in r-s space

Interpolation functions for a 3D Element in r-s-t space

$$h_1 = g_1 - (g_9 + g_{12} + g_{17})/2 \qquad\qquad h_1 = g_1 - (g_9 + g_{12} + g_{17})/2$$

$$h_1 = g_1 - (g_9 + g_{12} + g_{17})/2 \qquad\qquad h_1 = g_1 - (g_9 + g_{12} + g_{17})/2$$

$$h_1 = g_1 - (g_9 + g_{12} + g_{17})/2 \qquad\qquad h_1 = g_1 - (g_9 + g_{12} + g_{17})/2$$

$$h_1 = g_1 - (g_9 + g_{12} + g_{17})/2 \qquad\qquad h_j = g_j \text{ for } j = 9 - 20$$

$$h_1 = g_1 - (g_9 + g_{12} + g_{17})/2$$

$$h_1 = 0 \text{ if node } i \text{ is not included; otherwise,}$$

$$h_1 = G(r.r_i)G(s.s_i)G(t.t_i)$$

$$G(w.w_i) = \frac{1}{2}(1 + ww_i) \text{ for } w_i = \pm 1, \qquad w = r, s, t$$

$$G(w.w_i) = \frac{1}{2}(1 + w^2) \text{ for } w_i = 0, \qquad w = r, s, t$$

Table 3: Interpolation functions for a 3D Element in r-s-t space

For the case of a 2D axisymmetric revolution to model a 3D sphere, the 2D interpolation functions shall be used. Figure 12 is a graphical representation of the mapping described above.
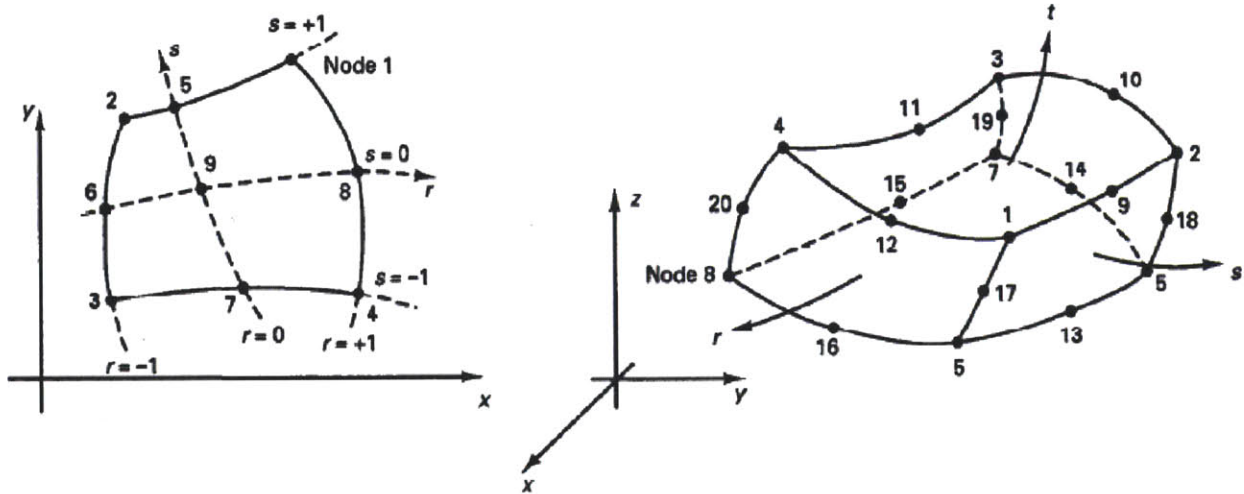
Figure 12: Isoparametric mapping for a 2D and 3D finite element

ELEMENTS OF CONSIDERATION

4-U NODE ELEMENT

The 4-U element is a displacement based element for 2D analysis and utilizes four nodes. This node allows the computation to become less expensive but the convergence rate is weaker. Due to the linear interpolation of this element, it requires more elements to represent bending behavior in beams or floor systems.

9-U NODE ELEMENT

The 9-U 2D Element is a displacement based element for 2D analysis and utilizes 9 nodes. This node allows the computation to become more expensive but the convergence rate is faster. This is the recommended element in the ADINA package to simulate the bending of beams.

9/3-U/P NODE ELEMENT

The 9/3 U/P 2D Element is a mixed based element that decouples pressure with displacement degrees of freedom. Because there are more degrees of freedom, the computation is more expensive than displacement based elements. However, for nearly incompressible isotropic materials, the U/P element has proven to be very useful as opposed to displacement based elements. The large increase in the bulk modulus of the material does not affect the strain energy of this formulation. This element can be used for 2D plane strain and axisymmetric behavior but not for plane stress.

4/1-U/P NODE ELEMENT

The 4/1 U/P 2D Element is the coarsest mixed based element that decouples pressure with displacement degrees of freedom. This element behaves under the same guidelines as the 9/3 U/P element but with some noticeable differences. There is only one pressure node which may lead to spurious energy problems if not properly used. This pressure node is either calculated as

"floating" and the interpolation field is taken as 1, or the node is chosen as the 9th interpolation location in the center of the element (Moaveni).

CONVERGENCE LAWS

LINEAR CONVERGENCE

For a continuum solid body, a solution to the variational formulation of the problem will equal to the exact solution of the physical model. If a finite element analysis is used and the variational formulation is discretized, the solution of the FEA regarding the displacements will be smaller. If a finer mesh is used, the solution will achieve a closer approximation to the physical model. It is shown that this convergence for a linear analysis is monotonic.

The following is the principle of virtual displacements for a continuum body

$$\int_V \bar{\varepsilon}^T \tau \, dV = \int_V \overline{U}^T f^B \, dV + \int_{S_f} \overline{U}^{S_f^T} f^{S_f} \, dS_f$$

As a shorthanded notation, the left hand side shall be rewritten as:

$$\int_V \bar{\varepsilon}^T \tau \, dV = a(u, u) = E = \text{Strain Energy Of Continuum}$$

The left hand side can be recognized as twice the strain energy of the continuum mathematical model and u is labeled as the exact solution. If the principle of virtual displacements is discretized by a finite element solution, the strain energy of the finite element solution shall be equal to:

$$\int_V \bar{\varepsilon}^T \tau \, dV = a(u_h, u_h) = E = \text{Strain Energy of FEA with element measure "h"}$$

The left hand side can be recognized as twice the strain energy of the finite element model with mesh measure "h" and u_h is labeled as the solution to this finite element model. For linear analysis, the solution of the finite element analysis with element measure "h" will have a monotonic convergence to the solution of the continuum mathematical model. Thus, twice the strain energy of the FEA model will always be smaller and will converge to the twice the strain energy of the continuum mathematical model.

$$2a(u, u) \geq 2a(u_h, u_h)$$

This property is extremely valuable because it provides us with a measuring tool to see if a given finite element analysis does or does not have a fine enough mesh for a given tolerable error in solution.

To use this tool properly, the following rules must apply (Bathe):

- The inherent geometry of the finer mesh model must use the identical geometry of the previous model and that the previous mesh mush be contained within the finer mesh.

$$V_h^1 \in V_h^2 \in \cdots \in V_h^i \in \cdots \in V$$

- The stress strain law is properly used.
- The constitutive relation C must be the same used in the continuum mathematical model.
- Compatibility of the mesh needs to be satisfied.

For a linear analysis, the strain energy converges with an order of ch2k

$$E - E_h \cong Ch^{2k}$$

An example of this monotonic convergence behavior is shown below for a given setting.
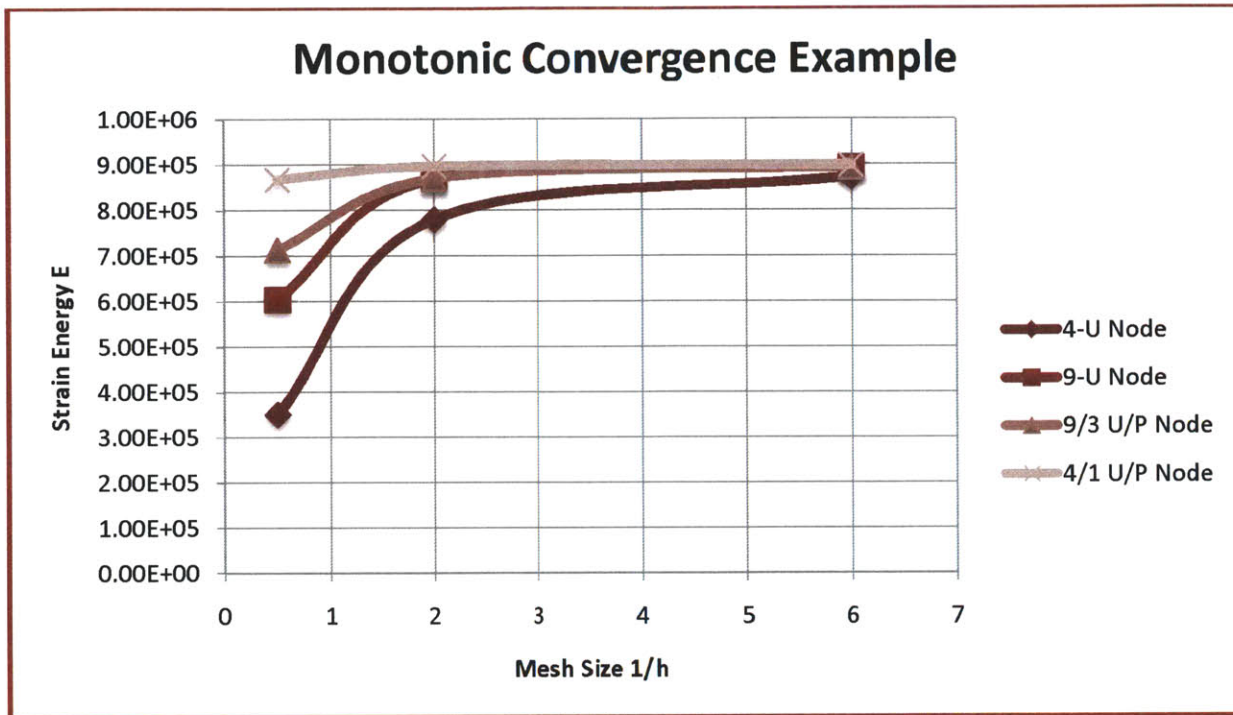
Figure 13: Monotonic Convergence Example

If a series of finer mesh strain energies are plotted in logarithmic space, the plot will be approximately linear with a slope of 2k. This shall be the measure of convergence. Because we do not know the exact strain energy E of the continuum mathematical model, a replacement must be made. For this analysis, E will be assumed to be equivalent to a very fine mesh E_h where E_h is the mesh implementing $1/h = 6$, and two smaller meshes of $1/h = 0.5$ and 2.

Finally it should be understood that for the U/P element formulation, convergence is assured because the analysis is linear, but the convergence may or may not converge monotonically. Therefore, the 2k law may not be used for U/P elements.

40

The following shows graphically the inherent problems of the displacement based FEA for modeling nearly incompressible orthotropic media. As can be seen for nearly incompressible orthotropic conditions, the effective stress jumps are terrible indicating the poor performance of utilizing displacement based elements. The elements are locking and are producing erroneous results (Cook).
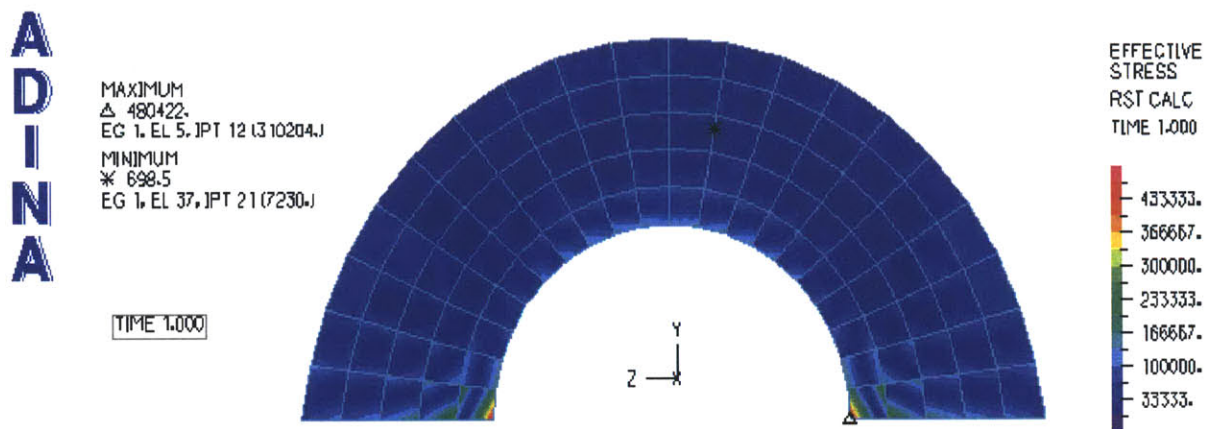
Figure 14: Effective Stress results for orthotropic nearly incompressible media
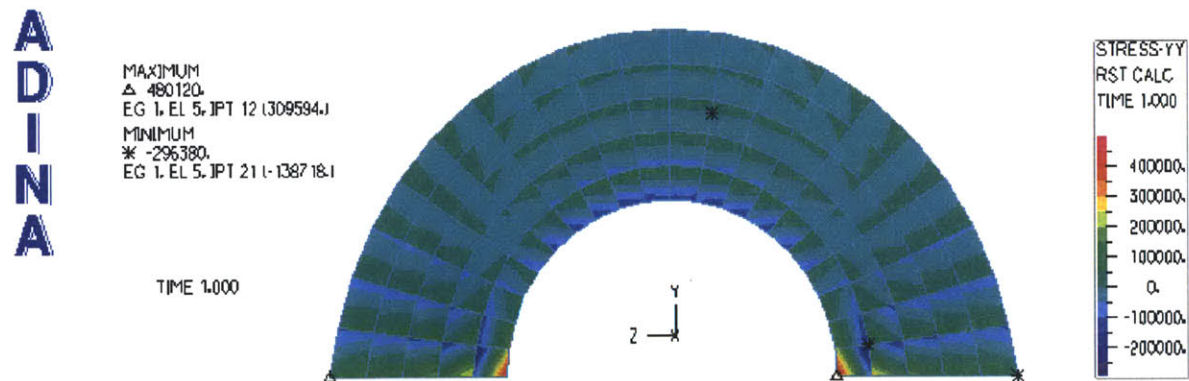
Figure 15: Global Y- Stress results for orthotropic nearly incompressible media

CHAPTER 4: FINITE ELEMENT ANALYSIS MODELING
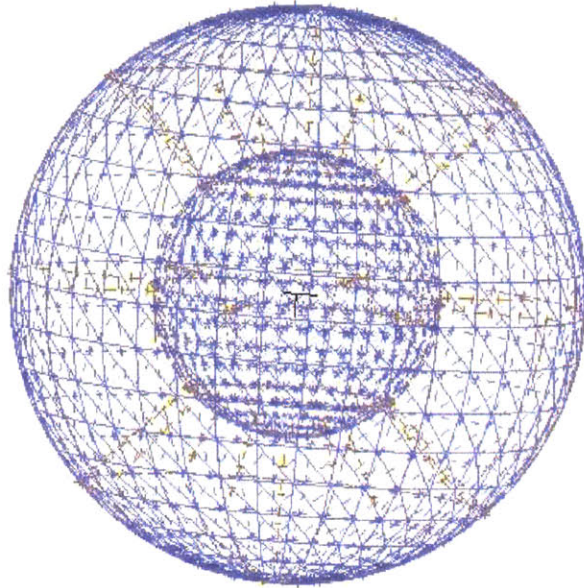
Figure 16: Experimental Model – 40 meter diameter sphere with 20 meter diameter fixed hollow core

This section shall discuss the experiment to be run that shall illustrate the superior performance of mixed U/P elements over displacement U elements regarding the analysis of a nearly incompressible linear orthotropic media subjected to an arbitrary loading.

EXPERIMENTAL MODEL

The model chosen to be used in this experiment is a 40 meter diameter sphere subjected to a uniform compressive load. This sphere includes a hollow 20 meter diameter core. The inner core of this sphere shall act as a fixed surface (All degrees of freedom on its surface are null). This geometry was chosen because of its high level of symmetry and its graphical display of incompressible media. The model is shown below.
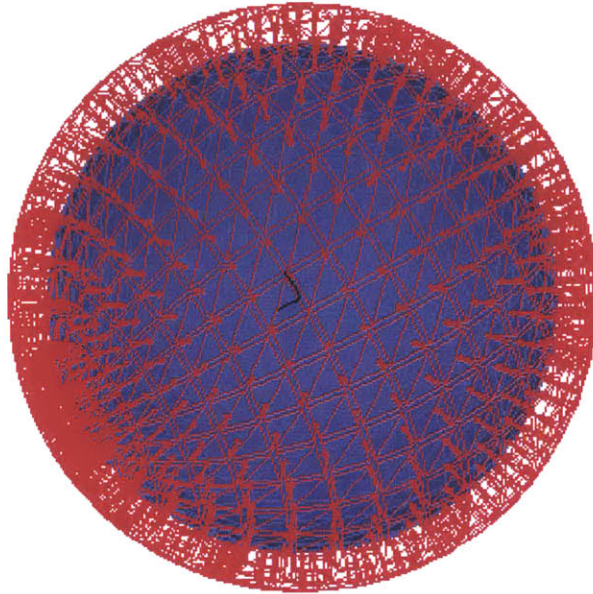
Figure 17: Experimental Model subjected to uniform compressive loading

Figure 16 shows a transparent view of the geometry of the sphere. The inner hollow core is easily displayed. Figure 17 displays the uniform compressive traction acting on the exterior surface. The purple mesh represents the applied stress field.

Recall that for an incompressible material, the volume of the material shall remain constant for any given time. Thus for the given geometry, a uniform compressive load acting on the outer surface of the sphere will not allow any deformation on its outer surface. Therefore, the outer surface area shall remain constant and the initial geometry shall be equivalent to the final geometry.

The size of the sphere chosen as 40 was made to allow the geometry to be entered in easily. With the center core, main points are defined by a distance of 10 apart. In ADINA, (the finite element program used to run the experiment) units are not defined. Throughout the rest of this text, no mention of units shall be given. However, all set units were based off of the English measuring system.

43

This philosophy holds in truth the main rule when applying a finite element analysis. "Garbage in. Garbage out". In short, the finite solution is not the exact solution to the real world physical problem. It is rather the solution to the mathematical model representing the physical problem. The "solution" will only expose the effects of the details the engineer has incorporated into the model. Ideally, if a floor beam is modeled mathematically as an isotropic material and the physical problem is an orthotropic material, the results will not display the effects of orthotropic behavior. Likewise, if a beam with a 1D beam element, it will not show me the stress distribution in classified Bernoulli and disturbed regions (Saint Variant's principle). With that said, one might argue that every finite element analysis should contain as much information as possible. i.e. everything should be modeled 3D with every screw, nut, bolt, and discontinuity accounted for with non-linear analysis. In a sense, this is a guaranteed solution that shows all effects from every element. But it is still only as good as the mathematical model (complex or not) and it is also very expensive to simulate and very tedious and time consuming to develop. The hierarchal finite element method philosophy teaches that the best model is not the most complex but rather the most effective in a hierarchal tabulation (Bucalem).

HIERARCHAL MODEL TABULATION

$$\left\{ \begin{array}{c} Hierarchal\ Model\ 1 \\ Hierarchal\ Model\ 2 \\ \dots\ \dots\ \dots\ \dots \\ \dots\ \dots\ \dots\ \dots \\ Hierarchal\ Model\ i \\ \dots\ \dots\ \dots\ \dots \\ \dots\ \dots\ \dots\ \dots \\ Hierarchal\ Model\ n \\ Continuum\ Body\ Solution \end{array} \right\}$$

The above shows the tabulated scheme of mathematical models in order of increasing complexity. As a model is chosen farther down the list, its "solution" will be closer and closer to the continuum body solution. However, as stated before this increase in solution convergence to modeling more accurate behavior is traded with increased expense of solution time and complexity in setting up a model. The engineer must never choose the penultimate finite element model because the setup time required and probability of mistakes in model entry will increase drastically. Instead, the engineer must choose the hierarchal model i such that the difference in solution performance from the next hierarchal model i+1 does not exceed a tolerance Δ, a value chosen by the modeler based on engineering judgment.

MODEL SYMMETRY

Below are two utilized hierarchal models that model this experiment. Using the argument of symmetry, it is shown how to move from model to a more simplistic version which is less computationally expensive and easier to control.

HIERARCHAL MODEL 1

For this project, the solid geometry was chosen to be such that the effects of compressive forces are symmetric throughout. Thus the following model was chosen. The inner core of the sphere is hollow and will act as a fixed boundary. This condition will allow the user to see the physical contraction of the element if compressible conditions are assumed. If a nearly incompressible situation arises, the displacement mesh in post processing should remain identical to the physical model (It does not move). To model this behavior, the boundary conditions will apply a fixed wall to the entire inner surface of the hollow sphere inside.

45
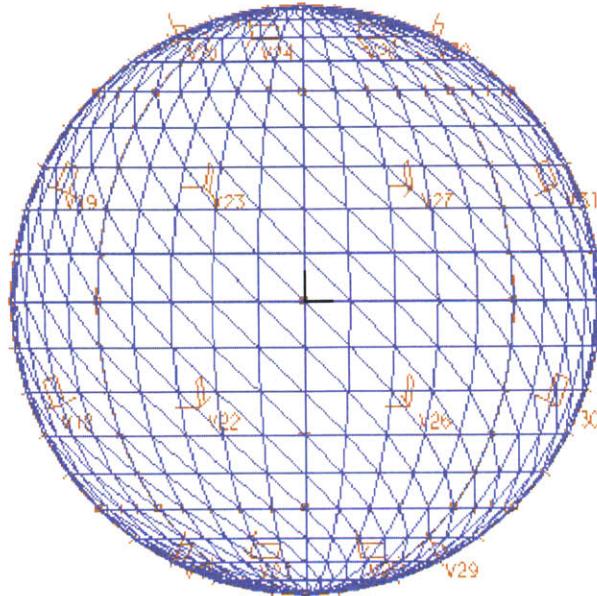
Figure 18: Hierarchal Model 1: 3D Hollow Sphere using 3D finite elements

This model consists of 53 points and 23 solid volumes to initialize the geometry. When a mesh of size h is applied, the number of nodes becomes rather large.

HIERARCHAL MODEL 2

Given the symmetry conditions of the above model, it is shown that to model this as an 2D axisymmetric cases is much more efficient. Due to symmetry conditions, it is assumed that for the axisymmetric case, the boundary conditions on the left inward boundary of the axisymmetric element are composed of fixity in the core and rollers at the end connections (Cook). This allows this model to contract with the same behavior as the hollowed solid sphere using 3D elements.
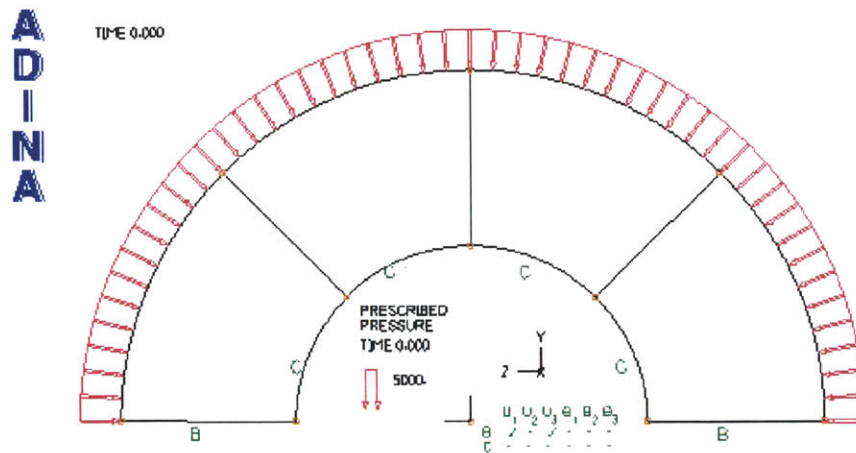
Figure 19: Hierarchical Model 2: Axisymmetric Hollow Sphere Revolution about Z-axis

Compared with hierarchical model 1, this axisymmetric model only needs 11 points and 4 surfaces to completely define its geometry. The revolution this 2D configuration creates completely models all effects from hierarchical model 1. The letters C and B represent the boundary conditions applied to the respective faces. The legend is shown in figure(). C represents fixed conditions with no degrees of freedom and B represents fixed translation in the Y axis.

MODELING WITH ADINA

The following is a detailed description of the modeling settings and properties within the ADINA program. ADINA stands for Automated Dynamic Iterative Nonlinear Analysis and was founded by Dr. Jurgen Klaus Bathe. This experiment maybe ran from any trusted finite element program but the initial configurations in ADINA are provided to guide the user. The geometry, surface structure, orthotropic conditions, and mesh sizes used are tabulated. The following procedure records the initial setup in ADINA. Tables include the values to be entered and screen captions of the related input windows are shown. For example, the heading configuration is shown below.

47

1 ThG: M.Eng. Thesis - Bateman

Table 4: Heading
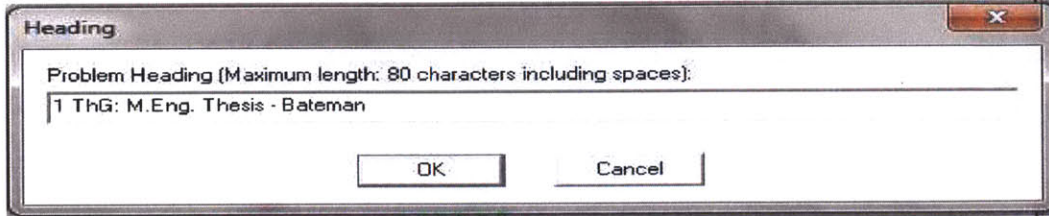
Figure 20: Adina Input - Heading

GEOMETRIC POINTS

The following are the points needed to define the geometry perimeter. Points 1-10 are based off of a cylindrical coordinate system centered at the origin, and point 11 is the Cartesian origin. Point 11 is needed as a reference to model the 8 arc lines that make the axisymmetric model. The system is the coordinate system used to describe the geometric placement of the point in ADINA. System 0 refers to the standard Cartesian global coordinate system and is the default setting. System 1 refers to the cylindrical coordinate transformation of the Cartesian global coordinate system.

Point Coordinates

Default Coordinate System: 0

	Point #	X1	X2	X3	System
1	1	10.0	-90.0	0.0	1
2	2	10.0	-45.0	0.0	1
3	3	10.0	0.0	0.0	1
4	4	10.0	45.0	0.0	1
5	5	10.0	90.0	0.0	1
6	6	20.0	-90.0	0.0	1
7	7	20.0	-45.0	0.0	1
8	8	20.0	0.0	0.0	1
9	9	20.0	45.0	0.0	1
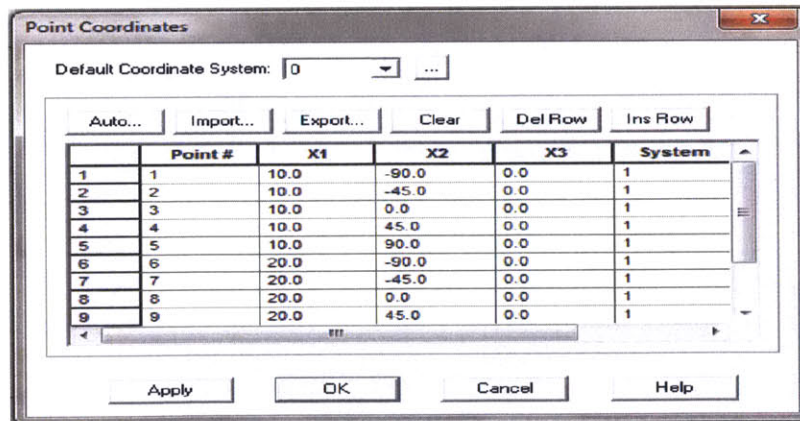
Figure 21: Adina Input – Point Coordinates

		Define Points		
Point #	X1	X2	X3	System
1	10	-90	0	1
2	10	-45	0	1
3	10	0	0	1
4	10	45	0	1
5	10	90	0	1
6	20	-90	0	1
7	20	-45	0	1
8	20	0	0	1
9	20	45	0	1
10	20	90	0	1
11	0	0	0	0

Table 5: Point Geometry

GEOMETRIC LINES AND SURFACES

For this model, only 4 surfaces are created. The surface layout was chosen to create a uniform mesh. These surfaces are created using the patch method which requires the labeling of the four line boundaries. There are two types of lines used to draw the desired geometry, straight and curved lines. The straight lines require two points to define and are labeled vertex. Curved lines require three points to define, two end points, and the center of the circle the arc is tracing. The table below records the necessary values. Each surface created will have its own coordinate system for meshing. In Adina, these directions are labeled by a small flag icon which appears in the center of each created surface. All surfaces must not have interior angles greater than 180 degrees otherwise the surfaces will not have a computed Jacobian matrix.

49

Define Arc Line			
Surface #	**Starting Point P1**	**End Point P2**	**Center**
1	1	2	11
2	2	3	11
3	3	4	11
4	4	5	11
5	6	7	11
6	7	8	11
7	8	9	11
8	9	10	11

Define Straight Line		
Line	**Vertex 1**	**Vertex 2**
9	1	6
10	2	7
11	3	8
12	4	9
13	5	10

Table 6: Adina Input – Geometric Lines and Surfaces

Define Surface				
Surface #	**Line 1**	**Line 2**	**Line 3**	**Line 4**
1	1	9	5	10
2	2	10	6	11
3	3	11	7	12
4	4	12	8	13

Table 7: Surface Geometry
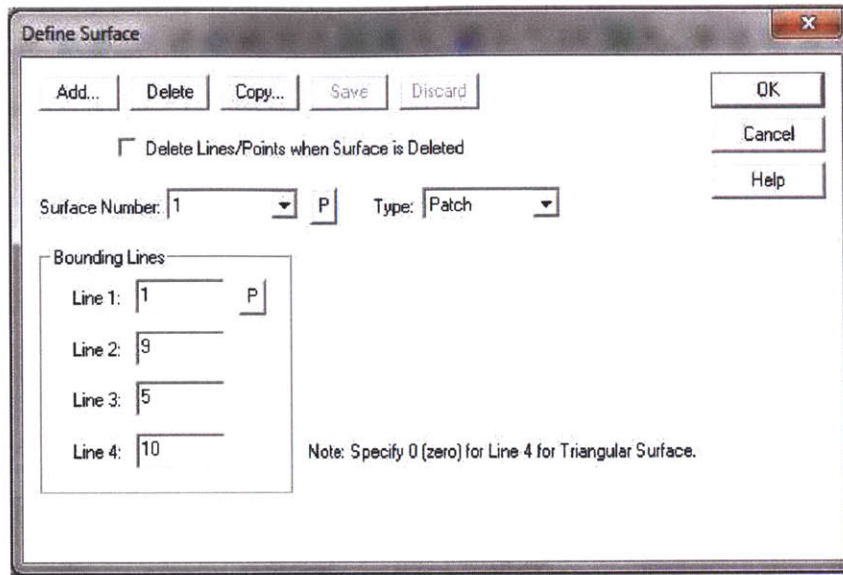
Figure 22: Adina Input – Define Surface

BOUNDARY CONDITIONS

As discussed in the symmetry section of this document, the boundary conditions call for a roller type connection which will allow rotation in every direction and translation in all but the global Y direction. Therefore, the following input creates the need restraint in ADINA. All other parameters not listed in the table such as temperature, warping, etc are also fixed.

Define Fixity						
Name	**X - Trans**	**Y - Trans**	**Z - Trans**	**X - Rot**	**Y - Rot**	**Z - Rot**
FIXED	X	X	X	X	X	X
YRoller		X		X	X	X
Apply Fixity						
Line 9, 13					**YRoller**	
Lines 1,2,3,4					**FIXED**	

Table 8: Boundary Conditions

51
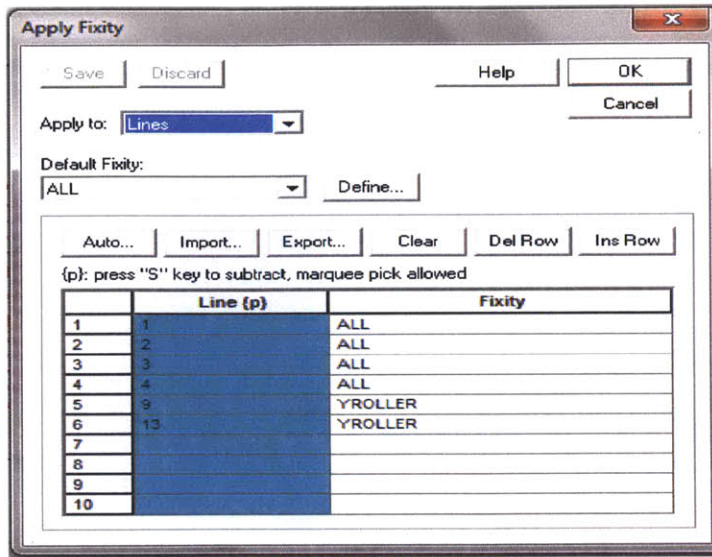
Figure 23: Adina Input – Apply Fixity

ORTHOTROPIC MATERIAL DEFINITIONS

The following details all material definitions in the experiment. The sphere will simulate twenty different material properties, most of them which are nearly incompressible situations. For this project, the Young's Modulus in each direction will be taken as a constant value of 20000 and the shear modulus shall be taken as a constant value of 10000. This eliminates the parameter E and G as variables from the restriction equations on Poisson's ratio. Thermal coefficients shall be taken as 0. Wrinkling shall not be modeled.

Manage Material Definitions						
Material: Elastic Linear Orthotropic						
E_A	E_B	E_C	v_{AB}	v_{AC}	v_{BC}	G_{AB}
30000	30000	30000	(Varies)	(Varies)	(Varies)	10000
Therm. A	Therm. B	Therm. C	G_{AB}	G_{AB}	Wrinkling	Density
0	0	0	0	0	No	0

Table 9: Material Definitions

52

Orthotropic Material Definitions

Material #	v_{AB}	v_{AC}	v_{BC}	Incompressible
1	0	0	0	N (Control)
2	0	0	0.5	N
3	0	0	0.999	Y
4	0	0.5	0	N
5	0	0.5	0.5	N
6	0	0.5	0.866	Y
7	0	0.999	0	Y
8	0	0.866	0.5	Y
9	0	0.707	0.707	Y
10	0.5	0	0	N
11	0.5	0	0.5	N
12	0.5	0	0.866	Y
13	0.5	0.5	0	N
14	0.5	0.866	0	Y
15	0.999	0	0	Y
16	0.866	0	0.5	Y
17	0.707	0	0.707	Y
18	0.866	0.5	0	Y
19	0.707	0.707	0	Y
20	0.499	0.499	0.499	Y(Isotropic)

Table 10: Orthotropic Material Definitions
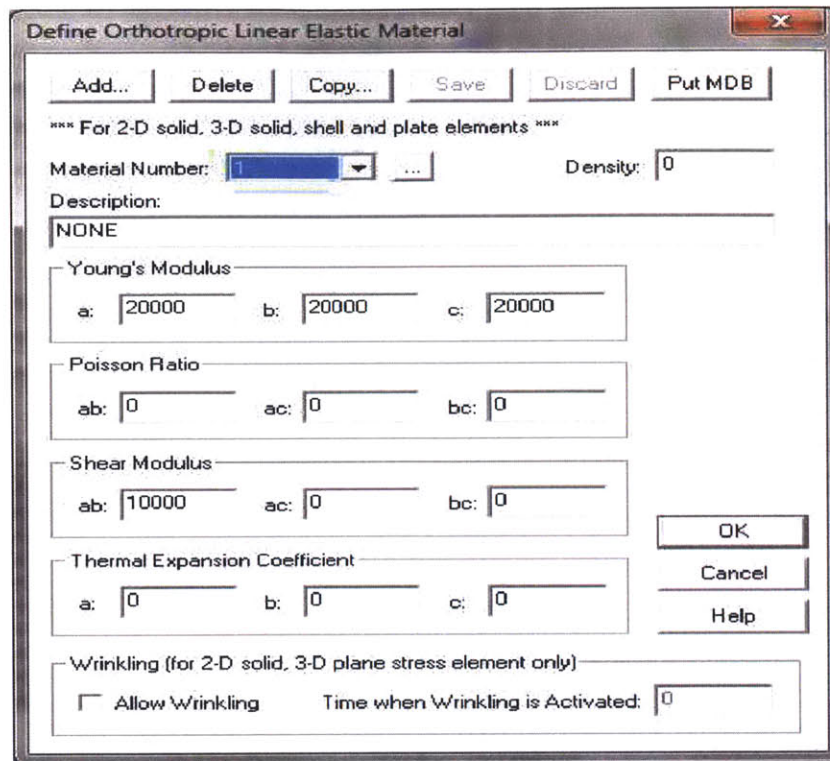
Figure 24: Adina Input – Define Orthotropic Linear Elastic Material

ELEMENT GROUP

Groups are grouped data to be applied when meshing a surface. Groups are a category scheme used in post processing to group areas of interest. The following group tells the program to mesh with axisymmetric 2D analysis, no incompatible modes, the material definitions (1-20) and small displacements and strains (linear analysis).

Define Element Group				
Group #	**Type**	**Element Sub Type**	**Default Material**	**Thickness**
1	2-D Solid	Axisymmetric	1	12

Table 11: Group Conditions
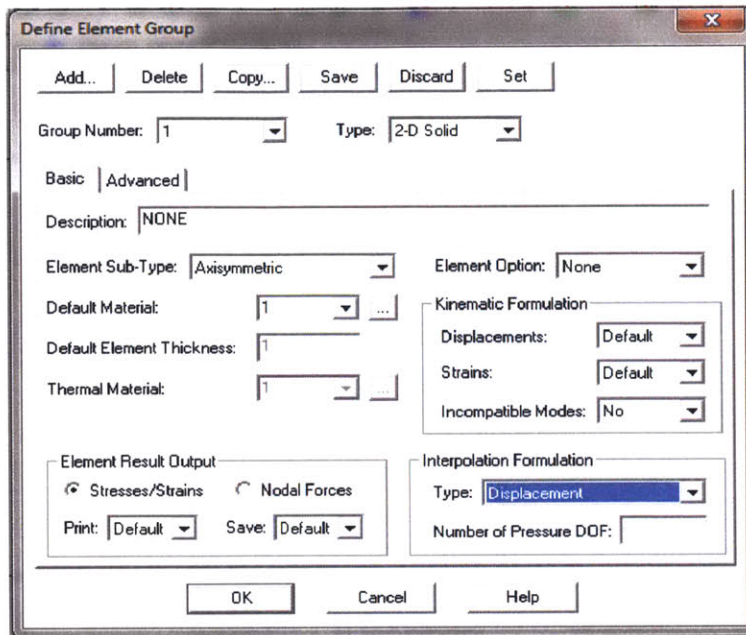
Figure 25: Adina Input – Define Element Group

LOADING

Loading on the sphere shall act as a uniform compressive load acting on the external surface area. For the axisymmetric 2D representation, this corresponds to lines 5,6,7, and 8.

Apply Load	
Pressure Number	**Magnitude**
1	1000
Line Number	**Pressure Load Number**
5	1
6	1
7	1
8	1

Table 12: Load Parameters
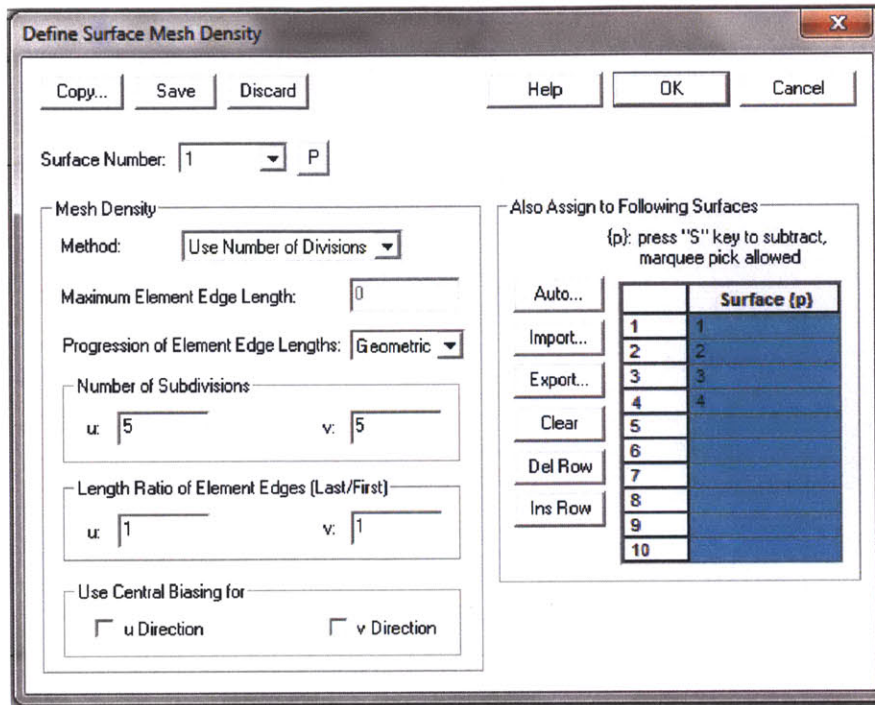
Figure 26: Adina Input – Define Surface Mesh Density

Define Surface Mesh Density

Mesh Size Measurement	Subdivisions u	Subdivisions v
1/h = 1/(10/5) = 0.5	5	5
1/h = 1/(10/20) = 2	20	20
1/h = 1/(10/60) = 6	60	60

Table 13: Mesh Density Parameters

Note: For this surface mesh, h = 5. When we refine the mesh for convergence check, we will use multiples of h. It is important that surfaces are meshed in the above order 3, 2, 1. If not, line 3 will not be meshed correctly.
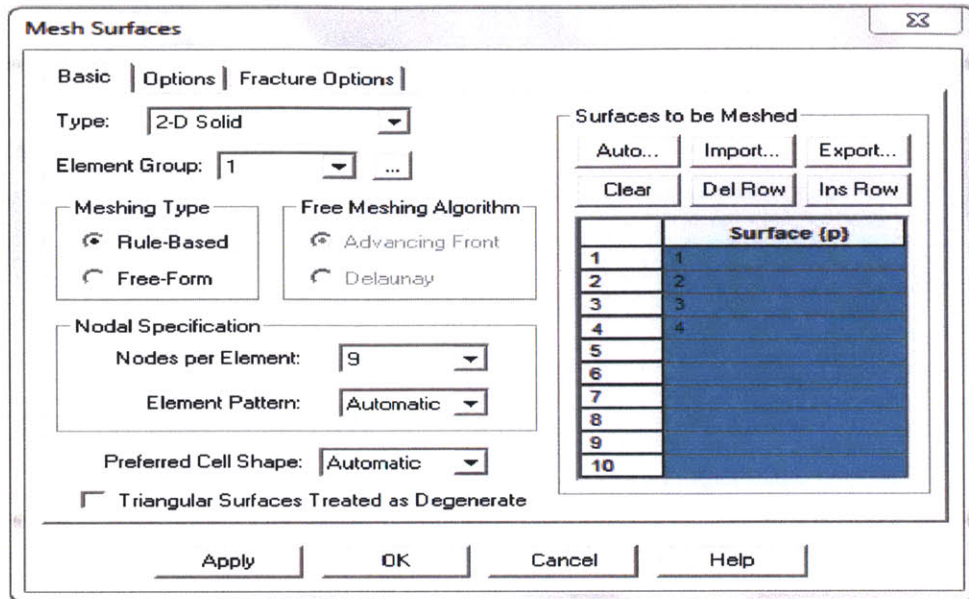
Figure 27: Adina Input – Mesh Surfaces

Mesh Surfaces

Surface #	Type	Element Group	Mesh Type	Node Specification
1	2-D Solid	1	Rule - Based	Varies
2	2-D Solid	1	Rule - Based	Varies
3	2-D Solid	1	Rule - Based	Varies
4	2-D Solid	1	Rule - Based	Varies

Table 14: Surface Parameters

RESULTS

CONVERGENCE RATE EVALUATION

For each of the cases, it is shown that all displacement based elements converge monotonically for all 20 material settings. U/P exhibit convergence but may not necessarily be monotonic Thus, it is heavily inferred that the constitutive effect on convergence is invariant of the choice between isotropic and orthotropic conditions.

TABLES AND GRAPHICS OF STRAIN ENERGY CONVERGENCE

The following list of tables tabulates the strain energy computed for each mesh size for each of the four elements subjected to the given defined material (Table 10). Poisson ratios used for each material are displayed as a heading. Logarithmic convergence only applies to the displacement based elements and is used to illustrate poor convergence. Following the list of tables are plotted values for each of the twenty materials.

Material 1	$v_{AB} = 0$			$v_{BC} = 0$		$v_{AC} = 0$
	Strain Energy vs. Mesh Size			Logarithmic Convergence		
Mesh Size	0.5	2	6	0.5	2	2k
4-U	6.94E+06	6.996E+06	6.999E+06	6.269E+04	3.354E+03	2.112E+00
9-U	7.000E+06	7.000E+06	7.000E+06	1.490E+02	6.000E-01	3.978E+00
4/1-U/P	6.943E+06	6.996E+06	7.000E+06	5.691E+04	3.206E+03	-
9/3-U/P	7.000E+06	7.000E+06	7.000E+06	1.038E+02	4.170E-01	-

Table 15: Material 1: vab = 0 vbc = 0 vac = 0

Material 2	$v_{AB} = 0$			$v_{BC} = 0$		$v_{AC} = 0.5$
	Strain Energy vs. Mesh Size			Logarithmic Convergence		
Mesh Size	0.5	2	6	0.5	2	2k
4-U	4.39E+06	4.430E+06	4.433E+06	4.650E+04	2.522E+03	2.102E+00
9-U	4.436E+06	4.433E+06	4.433E+06	-3.163E+03	-1.848E+02	2.048E+00
4/1-U/P	4.390E+06	4.430E+06	4.433E+06	4.285E+04	2.416E+03	-
9/3-U/P	4.436E+06	4.433E+06	4.433E+06	-3.254E+03	-1.857E+02	-

Table 16: Material 2: vab = 0 vbc = 0 vac = 0.5

Material 3	v_{AB} = 0			v_{BC} = 0		v_{AC} = 0.999
	Strain Energy vs. Mesh Size			Logarithmic Convergence		
Mesh Size	0.5	2	6	0.5	2	2k
4-U	3.51E+05	7.795E+05	8.717E+05	5.207E+05	9.214E+04	1.249E+00
9-U	6.046E+05	8.686E+05	8.934E+05	2.888E+05	2.480E+04	1.771E+00
4/1-U/P	8.675E+05	8.964E+05	8.981E+05	3.063E+04	1.699E+03	-
9/3-U/P	7.138E+05	8.693E+05	8.934E+05	1.797E+05	2.410E+04	-

Table 17: Material 3: vab = 0 vbc = 0 vac = 0.999

Material 4	v_{AB} = 0			v_{BC} = 0.5		v_{AC} = 0
	Strain Energy vs. Mesh Size			Logarithmic Convergence		
Mesh Size	0.5	2	6	0.5	2	2k
4-U	5.48E+06	5.514E+06	5.517E+06	4.030E+04	2.155E+03	2.113E+00
9-U	5.516E+06	5.517E+06	5.517E+06	6.440E+02	2.912E+01	2.233E+00
4/1-U/P	5.485E+06	5.515E+06	5.517E+06	3.220E+04	1.811E+03	-
9/3-U/P	5.516E+06	5.517E+06	5.517E+06	5.996E+02	2.894E+01	-

Table 18: Material 4: vab = 0 vbc = 0.5 vac = 0

Material 5	v_{AB} = 0			v_{BC} = 0.5		v_{AC} = 0.5
	Strain Energy vs. Mesh Size			Logarithmic Convergence		
Mesh Size	0.5	2	6	0.5	2	2k
4-U	2.64E+06	2.661E+06	2.662E+06	2.136E+04	1.148E+03	2.109E+00
9-U	2.663E+06	2.663E+06	2.663E+06	1.315E+02	2.609E+00	2.828E+00
4/1-U/P	2.645E+06	2.662E+06	2.663E+06	1.805E+04	1.012E+03	-
9/3-U/P	2.663E+06	2.663E+06	2.663E+06	7.781E+01	2.193E+00	-

Table 19: Material 5: vab = 0 vbc = 0.5 vac = 0.5

Material 6	v_{AB} = 0			v_{BC} = 0.5		v_{AC} = 0.866
	Strain Energy vs. Mesh Size			Logarithmic Convergence		
Mesh Size	0.5	2	6	0.5	2	2k
4-U	4.90E+03	4.968E+04	1.173E+05	1.124E+05	6.764E+04	3.664E-01
9-U	1.626E+05	1.956E+05	1.970E+05	3.437E+04	1.396E+03	2.311E+00
4/1-U/P	1.903E+05	1.967E+05	1.970E+05	6.792E+03	3.921E+02	-
9/3-U/P	1.985E+05	1.972E+05	1.971E+05	-1.424E+03	-7.881E+01	-

Table 20: Material 6: vab = 0 vbc = 0.5 vac = 0.866

Material 7	v_{AB} = 0			v_{BC} = 0.999		v_{AC} = 0
	Strain Energy vs. Mesh Size			Logarithmic Convergence		
Mesh Size	0.5	2	6	0.5	2	k
4-U	1.39E+05	2.156E+05	2.243E+05	8.525E+04	8.712E+03	1.645E+00
9-U	3.192E+05	2.385E+05	2.283E+05	-9.093E+04	-1.021E+04	1.577E+00
4/1-U/P	2.291E+05	2.263E+05	2.261E+05	-2.915E+03	-1.402E+02	-
9/3-U/P	3.606E+05	2.390E+05	2.283E+05	-1.323E+05	-1.070E+04	-

Table 21: Material 7: vab = 0 vbc = 0.999 vac = 0

Material 8	v_{AB} = 0			v_{BC} = 0.866		v_{AC} = 0.5
	Strain Energy vs. Mesh Size			Logarithmic Convergence		
Mesh Size	0.5	2	6	0.5	2	2k
4-U	9.69E+02	5.522E+03	9.528E+03	8.559E+03	4.007E+03	5.475E-01
9-U	1.289E+04	1.379E+04	1.377E+04	8.776E+02	-1.908E+01	#NUM!
4/1-U/P	1.377E+04	1.375E+04	1.375E+04	-2.325E+01	2.130E-01	-
9/3-U/P	1.721E+04	1.397E+04	1.378E+04	-3.429E+03	-1.829E+02	-

Table 22: Material 8: vab = 0 vbc = 0.866 vac = 0.5

Material 9	v_{AB} = 0			v_{BC} = 0.707		v_{AC} = 0.707
	Strain Energy vs. Mesh Size			Logarithmic Convergence		
Mesh Size	0.5	2	6	0.5	2	2k
4-U	1.24E+04	4.321E+04	5.874E+04	4.636E+04	1.553E+04	7.889E-01
9-U	6.505E+04	6.708E+04	6.716E+04	2.110E+03	7.266E+01	2.430E+00
4/1-U/P	6.530E+04	6.704E+04	6.715E+04	1.853E+03	1.076E+02	-
9/3-U/P	6.717E+04	6.716E+04	6.716E+04	-6.511E+00	-1.498E-01	-

Table 23: Material 9: vab = 0 vbc = 0.707 vac = 0.707

Material 10	v_{AB} = 0.5			v_{BC} = 0		v_{AC} = 0
	Strain Energy vs. Mesh Size			Logarithmic Convergence		
Mesh Size	0.5	2	6	0.5	2	2k
4-U	4.38E+06	4.426E+06	4.428E+06	4.592E+04	2.552E+03	2.085E+00
9-U	4.427E+06	4.429E+06	4.429E+06	1.623E+03	8.483E+01	2.129E+00
4/1-U/P	4.386E+06	4.426E+06	4.429E+06	4.267E+04	2.503E+03	-
9/3-U/P	4.427E+06	4.429E+06	4.429E+06	1.549E+03	8.386E+01	-

Table 24: Material 10: vab = 0.5 vbc = 0 vac = 0

Material 11	v_{AB} = 0.5			v_{BC} = 0		v_{AC} = 0.5
	Strain Energy vs. Mesh Size			Logarithmic Convergence		
Mesh Size	0.5	2	6	0.5	2	2k
4-U	2.23E+06	2.250E+06	2.251E+06	1.932E+04	1.032E+03	2.113E+00
9-U	2.252E+06	2.252E+06	2.252E+06	-7.766E+02	-4.288E+01	2.089E+00
4/1-U/P	2.234E+06	2.251E+06	2.252E+06	1.760E+04	9.892E+02	-
9/3-U/P	2.252E+06	2.252E+06	2.252E+06	-7.927E+02	-4.294E+01	-

Table 25: Material 11: vab = 0.5 vbc = 0 vac = 0.5

Material 12	v_{AB} = 0.5			v_{BC} = 0		v_{AC} = 0.866
	Strain Energy vs. Mesh Size			Logarithmic Convergence		
Mesh Size	0.5	2	6	0.5	2	2k
4-U	2.28E+03	2.401E+04	6.029E+04	5.801E+04	3.628E+04	3.386E-01
9-U	7.663E+04	1.011E+05	1.023E+05	2.562E+04	1.153E+03	2.237E+00
4/1-U/P	9.864E+04	1.021E+05	1.023E+05	3.670E+03	2.143E+02	-
9/3-U/P	1.055E+05	1.025E+05	1.024E+05	-3.156E+03	-1.718E+02	-

Table 26: Material 12: vab = 0.5 vbc = 0 vac = 0.866

Material 13	v_{AB} = 0.5			v_{BC} = 0.5		v_{AC} = 0
	Strain Energy vs. Mesh Size			Logarithmic Convergence		
Mesh Size	0.5	2	6	0.5	2	2k
4-U	2.64E+06	2.661E+06	2.662E+06	2.150E+04	1.168E+03	2.101E+00
9-U	2.662E+06	2.662E+06	2.662E+06	2.332E+01	-1.978E+00	2.481E+00
4/1-U/P	2.644E+06	2.661E+06	2.662E+06	1.828E+04	1.043E+03	-
9/3-U/P	2.662E+06	2.662E+06	2.662E+06	-3.532E+01	-2.565E+00	-

Table 27: Material 13: vab = 0.5 vbc = 0.5 vac = 0

Material 14	v_{AB} = 0.5			v_{BC} = 0.866		v_{AC} = 0
	Strain Energy vs. Mesh Size			Logarithmic Convergence		
Mesh Size	0.5	2	6	0.5	2	2k
4-U	8.89E+02	2.661E+06	2.662E+06	2.661E+06	1.168E+03	5.577E+00
9-U	1.116E+04	1.395E+04	1.395E+04	2.786E+03	2.798E+00	4.980E+00
4/1-U/P	1.323E+04	1.386E+04	1.390E+04	6.734E+02	4.054E+01	-
9/3-U/P	2.025E+04	1.431E+04	1.397E+04	-6.274E+03	-3.355E+02	-

Table 28: Material 14: vab = 0.5 vbc = 0.866 vac = 0

Material 15	v_{AB} = 0.999		v_{BC} = 0		v_{AC} = 0	
	Strain Energy vs. Mesh Size			Logarithmic Convergence		
Mesh Size	0.5	2	6	0.5	2	2k
4-U	3.25E+05	7.35E+05	8.32E+05	5.07E+05	9.77E+04	1.188E+00
9-U	8.39E+05	8.58E+05	8.58E+05	1.95E+04	3.13E+02	2.979E+00
4/1-U/P	8.27E+05	8.56E+05	8.58E+05	3.04E+04	2.09E+03	-
9/3-U/P	8.589E+05	8.580E+05	8.581E+05	-8.327E+02	3.635E+01	-

Table 29: Material 15: vab = 0.999 vbc = 0 vac = 0

Material 16	v_{AB} = 0.866		v_{BC} = 0		v_{AC} = 0.5	
	Strain Energy vs. Mesh Size			Logarithmic Convergence		
Mesh Size	0.5	2	6	0.5	2	2k
4-U	2.10E+03	2.23E+04	5.67E+04	5.46E+04	3.44E+04	3.333E-01
9-U	9.45E+04	1.01E+05	1.01E+05	6.27E+03	2.51E+02	2.321E+00
4/1-U/P	9.76E+04	1.01E+05	1.01E+05	3.24E+03	1.95E+02	-
9/3-U/P	1.013E+05	1.009E+05	1.008E+05	-4.731E+02	-2.400E+01	-

Table 30: Material 16: vab = 0.866 vbc = 0 vac = 0.5

Material 17	v_{AB} = 0.707		v_{BC} = 0		v_{AC} = 0.707	
	Strain Energy vs. Mesh Size			Logarithmic Convergence		
Mesh Size	0.5	2	6	0.5	2	2k
4-U	1.18E+03	1.19E+03	1.19E+03	9.91E+00	5.25E-01	2.119E+00
9-U	1.41E+03	1.25E+03	1.20E+03	-2.16E+02	-4.80E+01	1.085E+00
4/1-U/P	1.18E+03	1.19E+03	1.19E+03	3.76E+00	4.78E-01	-
9/3-U/P	2.544E+03	1.273E+03	1.201E+03	-1.343E+03	-7.235E+01	-

Table 31: Material 17: vab = 0.707 vbc = 0 vac = 0.707

Material 18	v_{AB} = 0.866			v_{BC} = 0.5		v_{AC} = 0
	Strain Energy vs. Mesh Size			Logarithmic Convergence		
Mesh Size	0.5	2	6	0.5	2	2k
4-U	4.09E+03	4.38E+04	1.08E+05	1.04E+05	6.45E+04	3.463E-01
9-U	1.80E+05	1.94E+05	1.94E+05	1.44E+04	5.78E+02	2.320E+00
4/1-U/P	1.87E+05	1.94E+05	1.94E+05	6.63E+03	3.98E+02	-
9/3-U/P	1.946E+05	1.942E+05	1.942E+05	-4.922E+02	-2.449E+01	-

Table 32: Material 18: vab = 0.866 vbc = 0.5 vac = 0

Material 19	v_{AB} = 0.707			v_{BC} = 0.707		v_{AC} = 0
	Strain Energy vs. Mesh Size			Logarithmic Convergence		
Mesh Size	0.5	2	6	0.5	2	2k
4-U	1.12E+04	4.16E+04	5.80E+04	4.69E+04	1.65E+04	7.541E-01
9-U	6.35E+04	6.73E+04	6.73E+04	3.82E+03	5.03E+01	3.123E+00
4/1-U/P	6.50E+04	6.71E+04	6.73E+04	2.30E+03	1.36E+02	-
9/3-U/P	6.912E+04	6.741E+04	6.731E+04	-1.815E+03	-9.657E+01	-

Table 33: Material19: vab = 0.707 vbc = 0.707 vac = 0

Material 20	v_{AB} = 0.499			v_{BC} = 0.499		v_{AC} = 0.499
	Strain Energy vs. Mesh Size			Logarithmic Convergence		
Mesh Size	0.5	2	6	0.5	2	2k
4-U	1.74E+04	1.75E+04	1.75E+04	1.25E+02	6.68E+00	2.115E+00
9-U	1.75E+04	1.75E+04	1.75E+04	1.90E-01	1.42E-03	3.532E+00
4/1-U/P	1.74E+04	1.75E+04	1.75E+04	1.07E+02	6.00E+00	-
9/3-U/P	1.749E+04	1.749E+04	1.749E+04	4.599E-02	7.700E-04	-

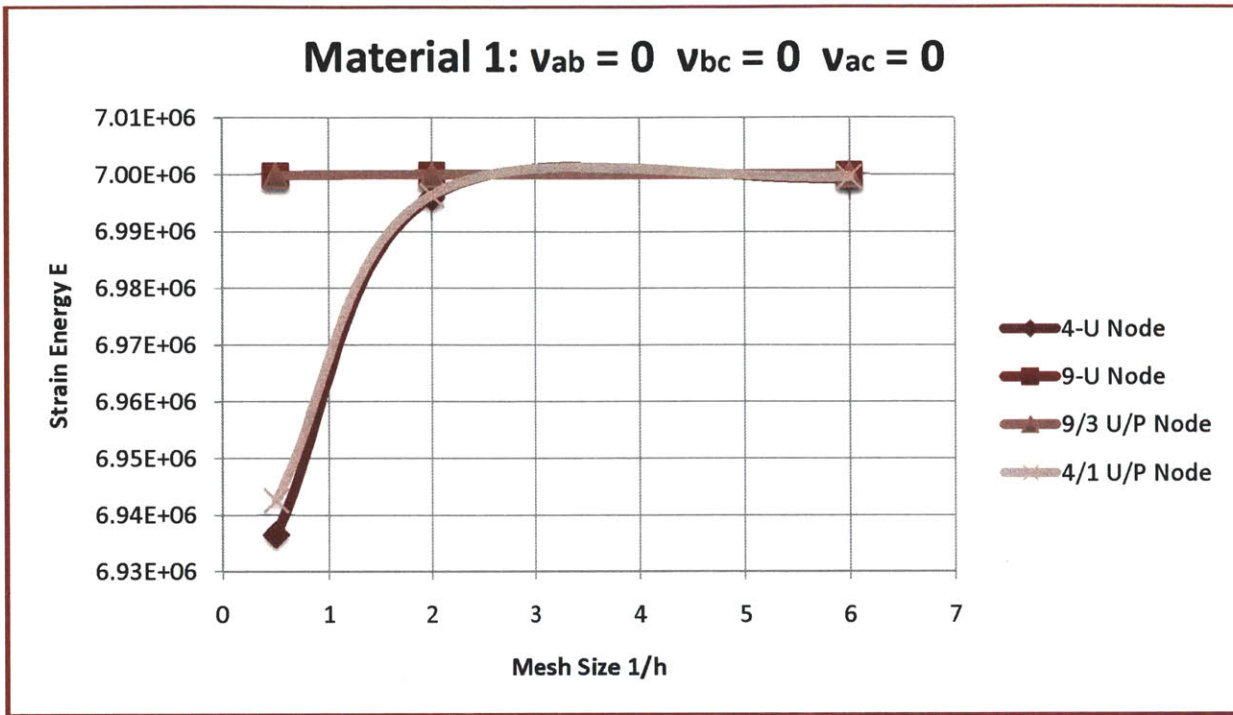Table 34: Material 20: vab = 0.499 vbc = 0.499 vac = 0.49
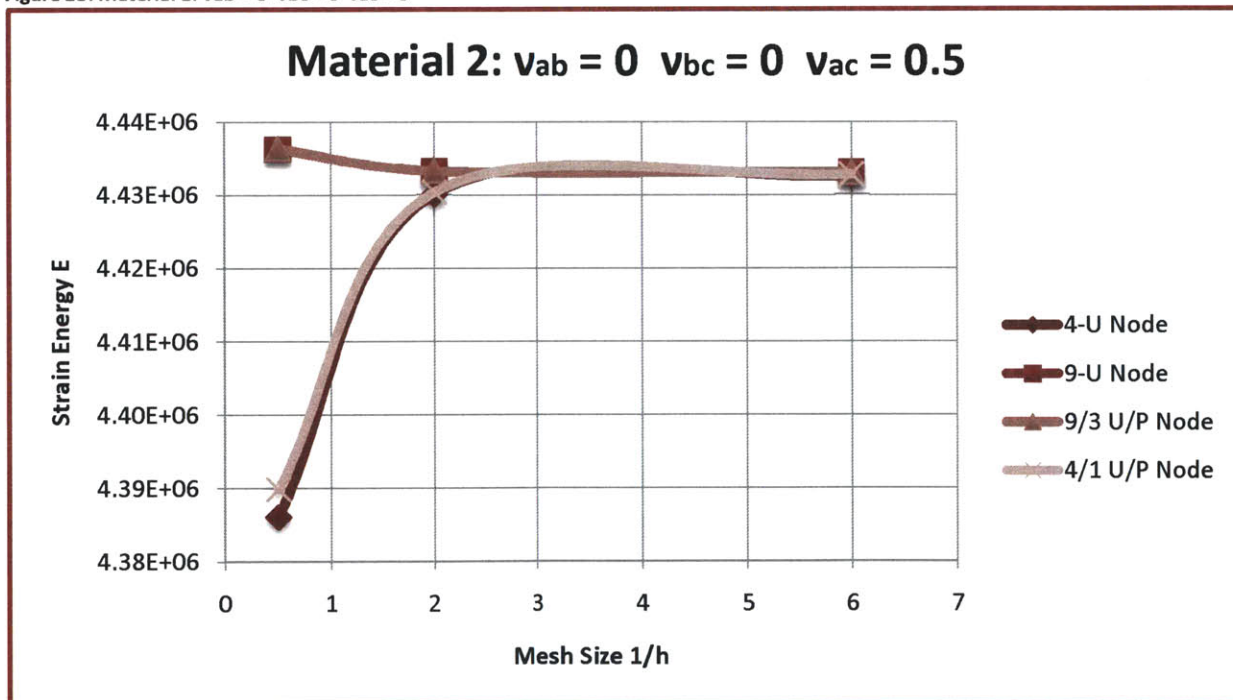
Figure 28: Material 1: vab = 0 vbc = 0 vac = 0
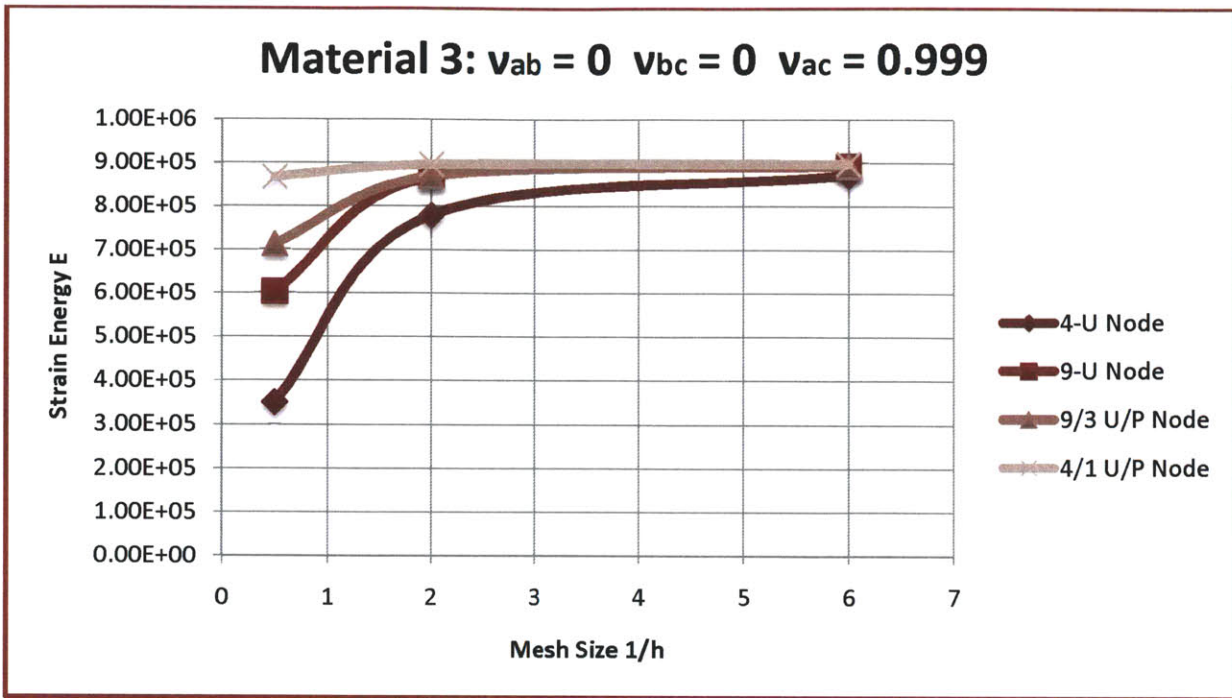

Figure 29: Material 2: vab = 0 vbc = 0 vac = 0.5

Figure 30: Material 3: vab = 0 vbc = 0 vac = 0.999
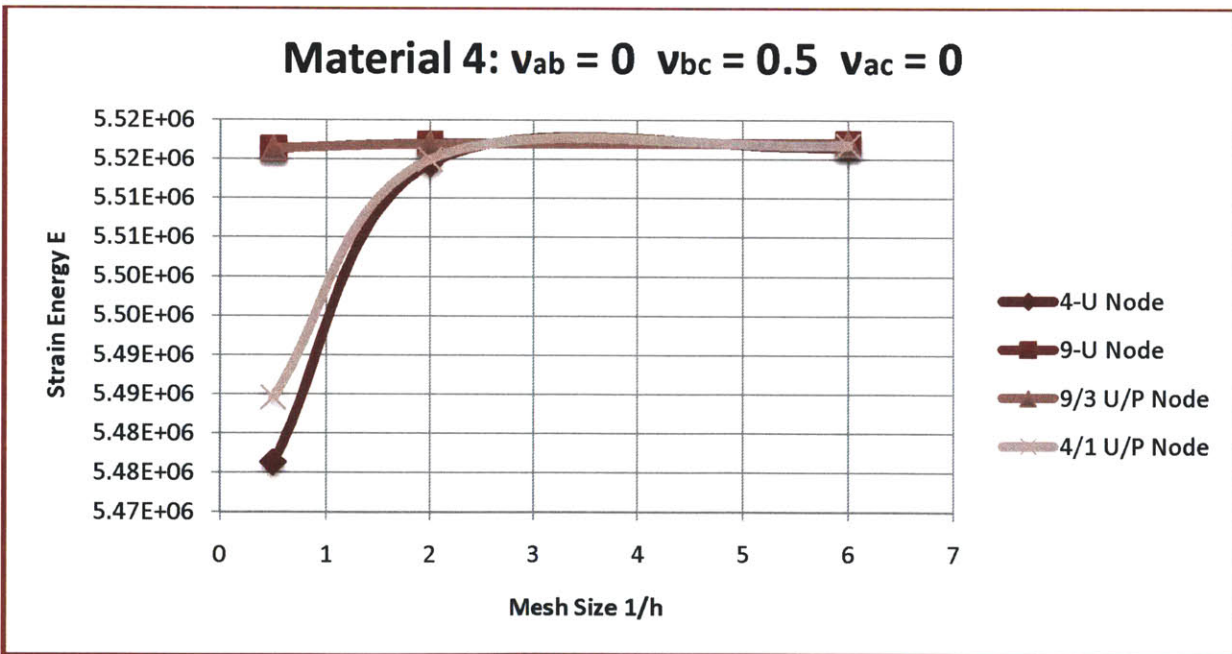
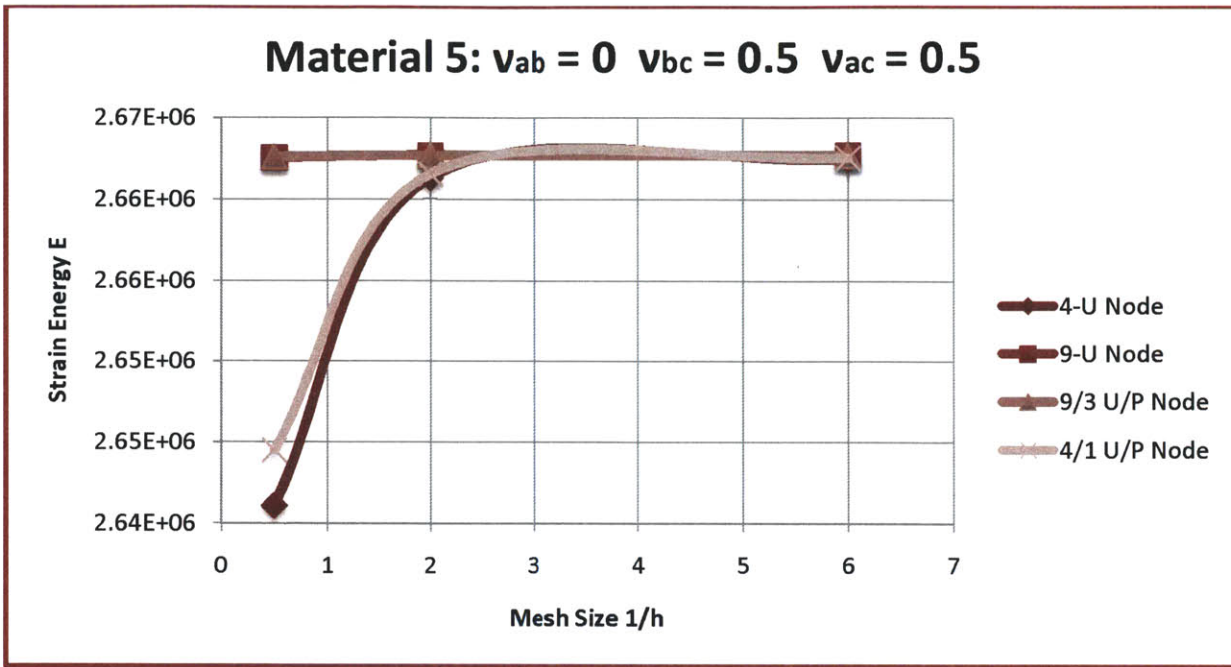Figure 31: Material 4: vab = 0 vbc = 0.5 vac = 0

Figure 32: Material 5: vab = 0 vbc = 0.5 vac = 0.5
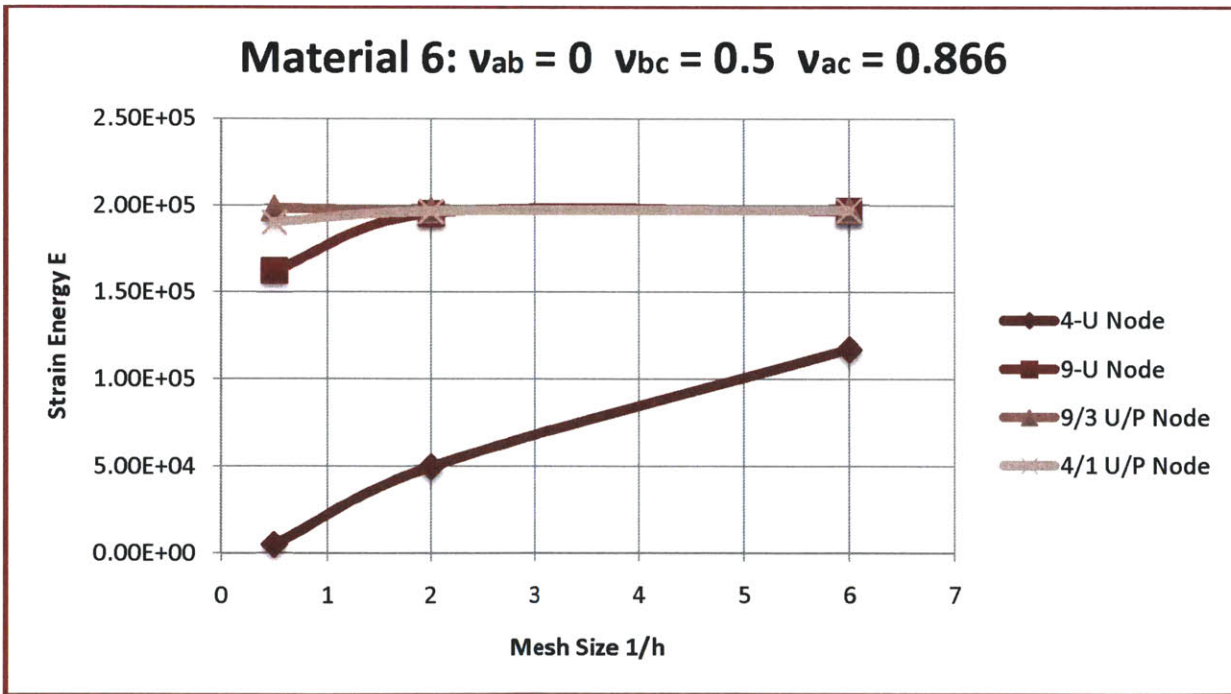
Figure 33: Material 6: vab = 0 vbc = 0.5 vac = 0.866
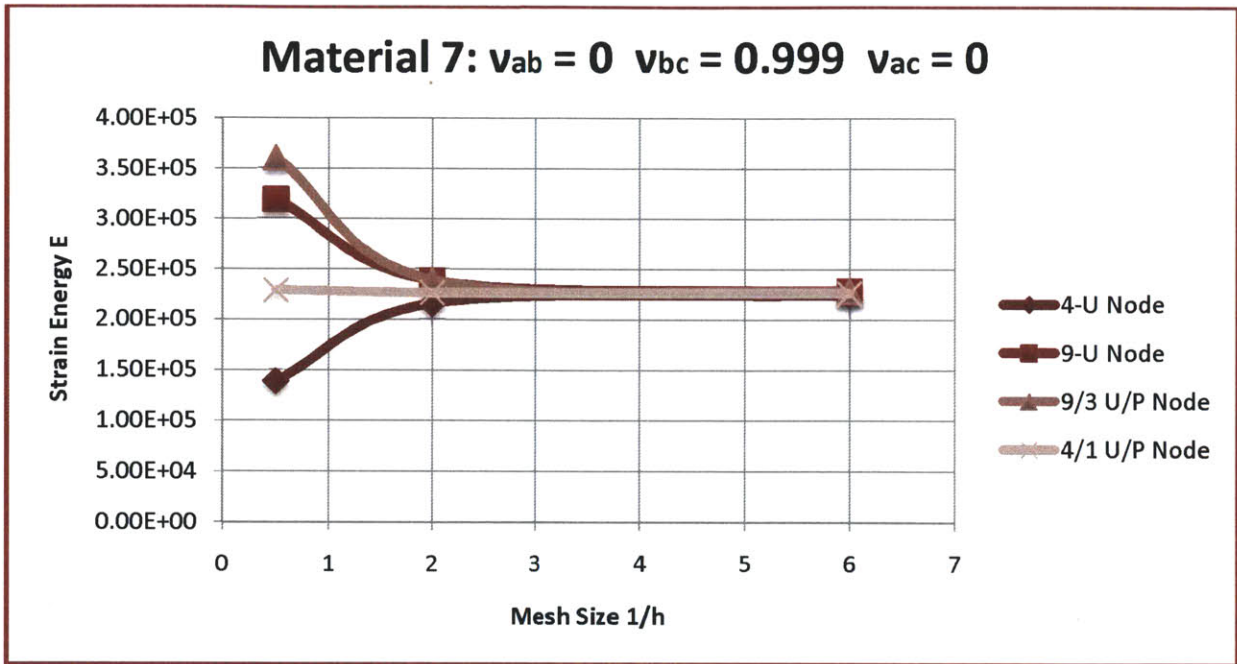
Figure 34: Material 7: vab = 0 vbc = 0.999 vac = 0
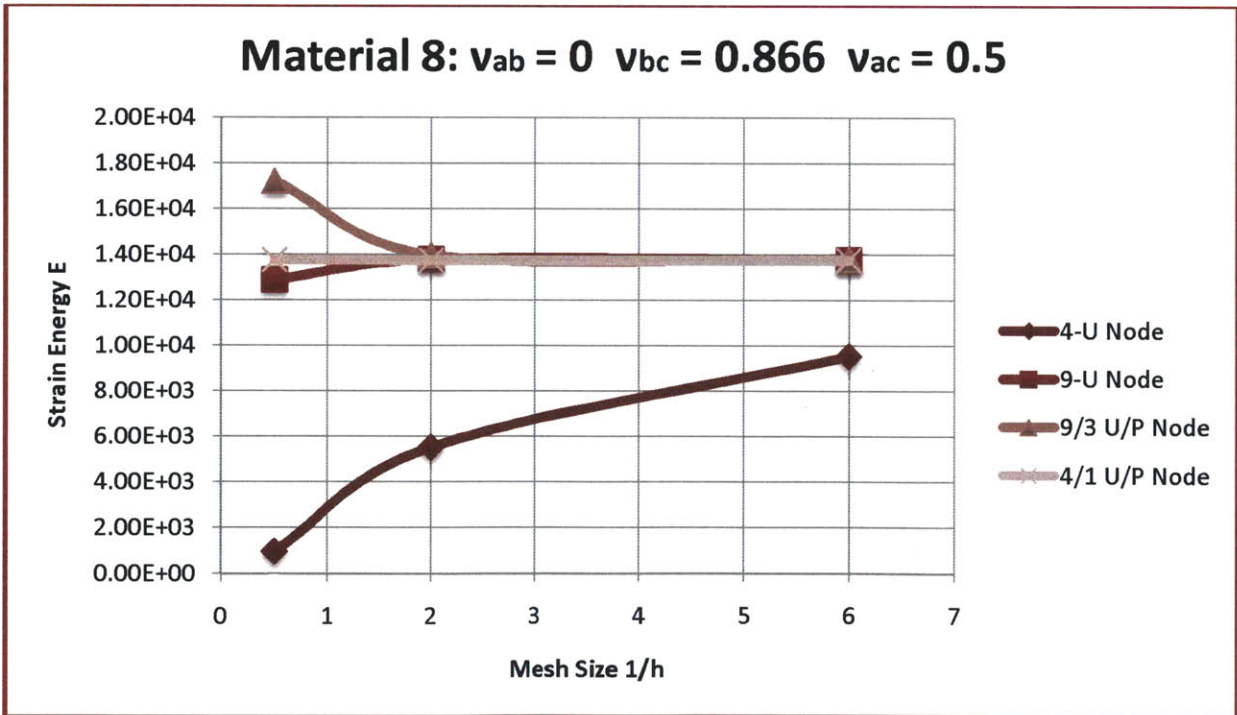
Figure 35: Material 8: vab = 0 vbc = 0.866 vac = 0.5

68
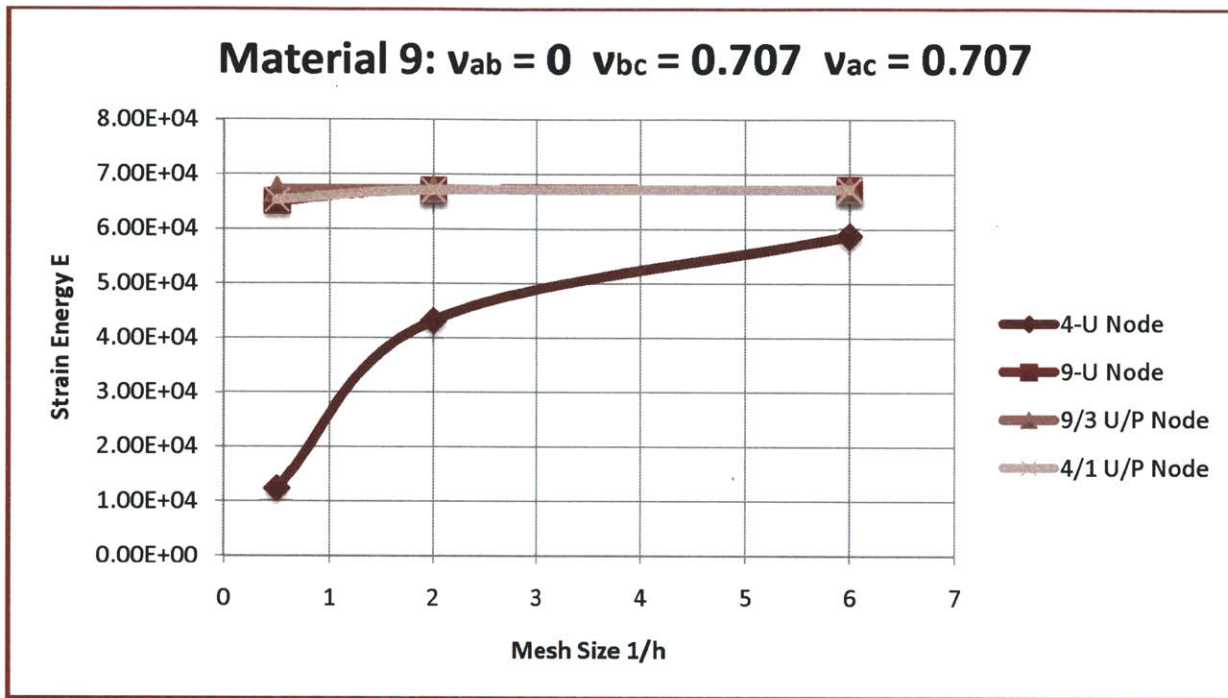
Figure 36: Material 9: vab = 0 vbc = 0.707 vac = 0.707
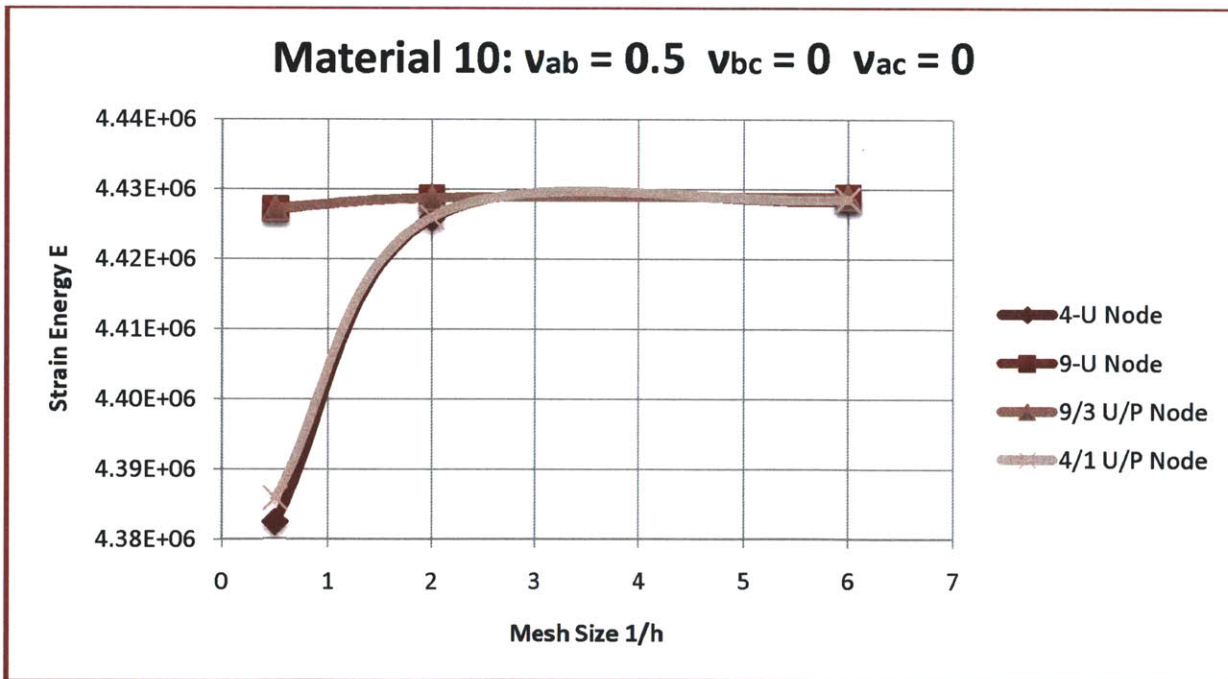
Figure 37: Material 10: vab = 0.5 vbc = 0 vac = 0

69
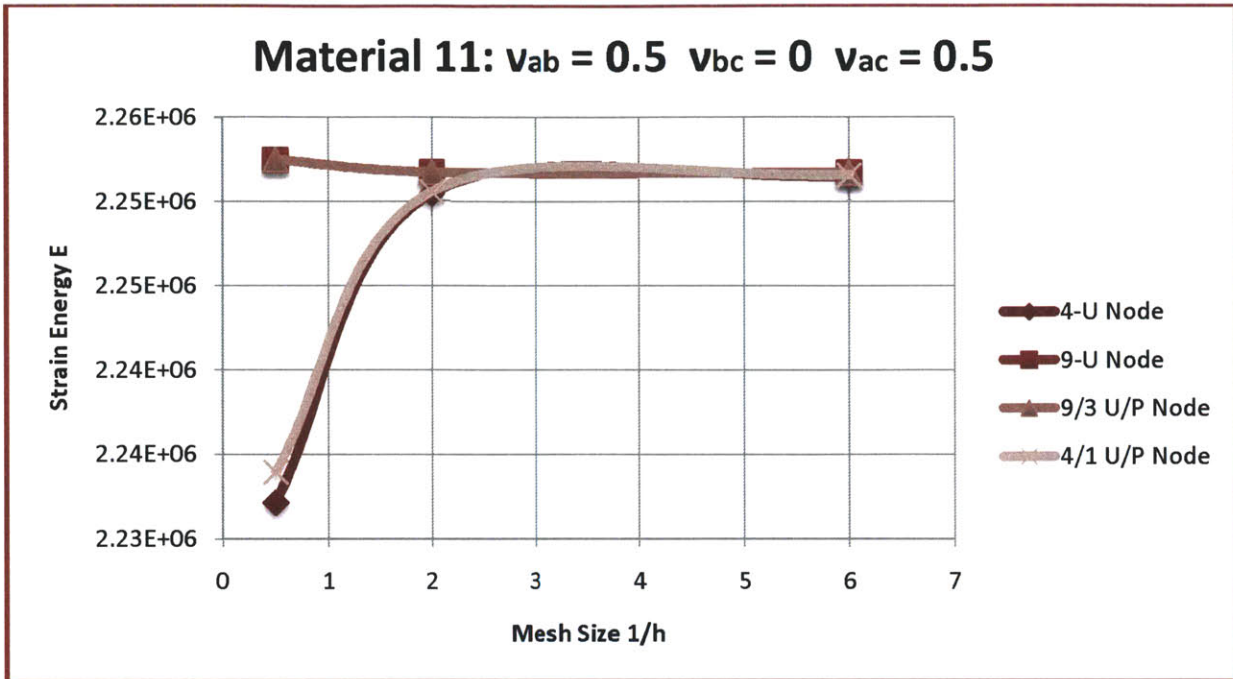
Figure 38: Material 11: vab = 0.5 vbc = 0 vac = 0.5
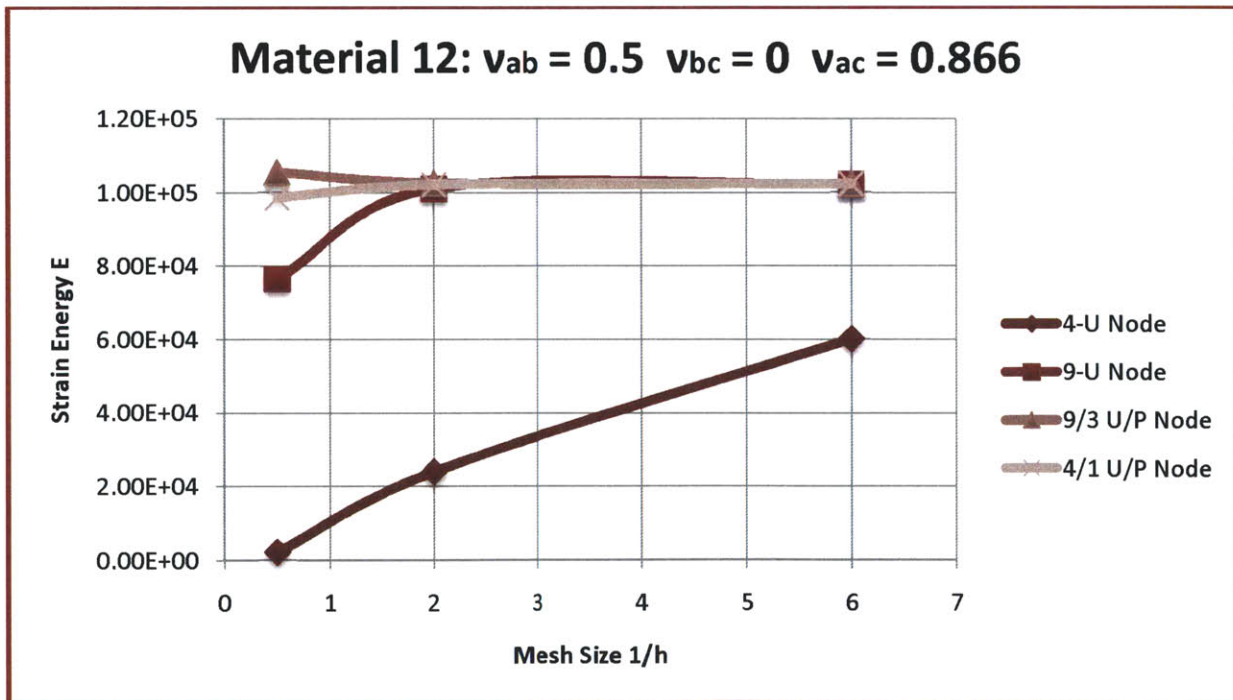
Figure 39: Material 12: vab = 0.5 vbc = 0 vac = 0.866

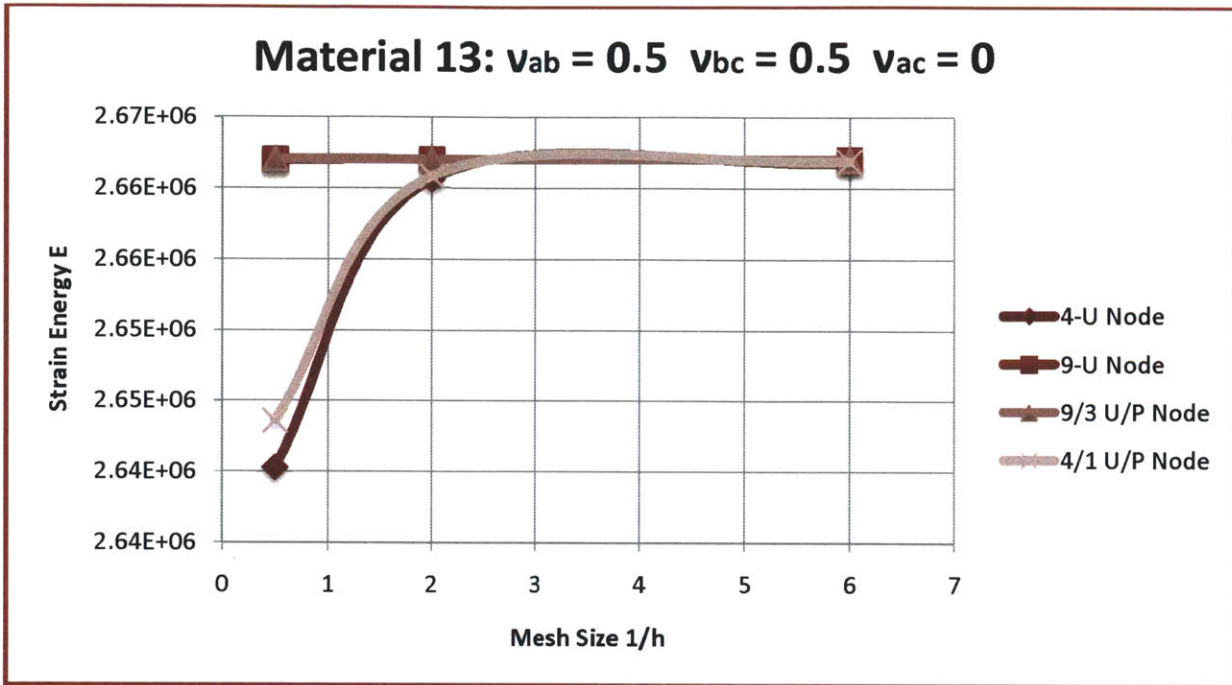**Figure 40: Material 13: vab = 0.5 vbc = 0.5 vac = 0**
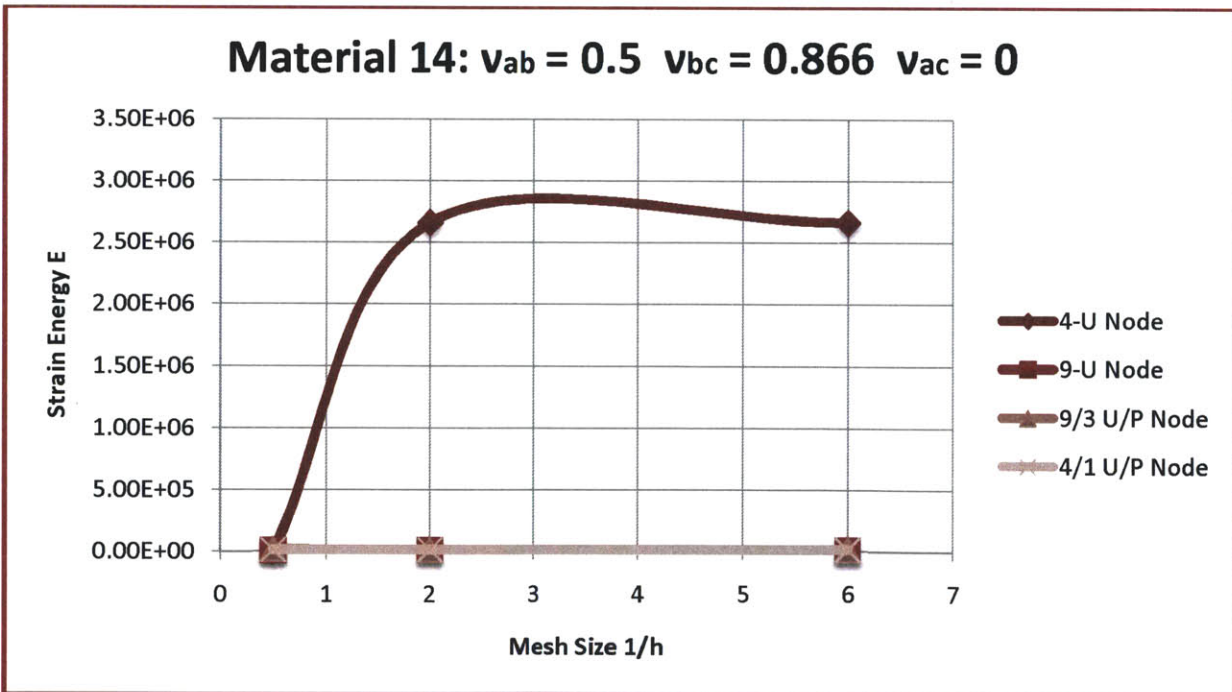
Figure 41: Material 14: vab = 0.5 vbc = 0.866 vac = 0

71
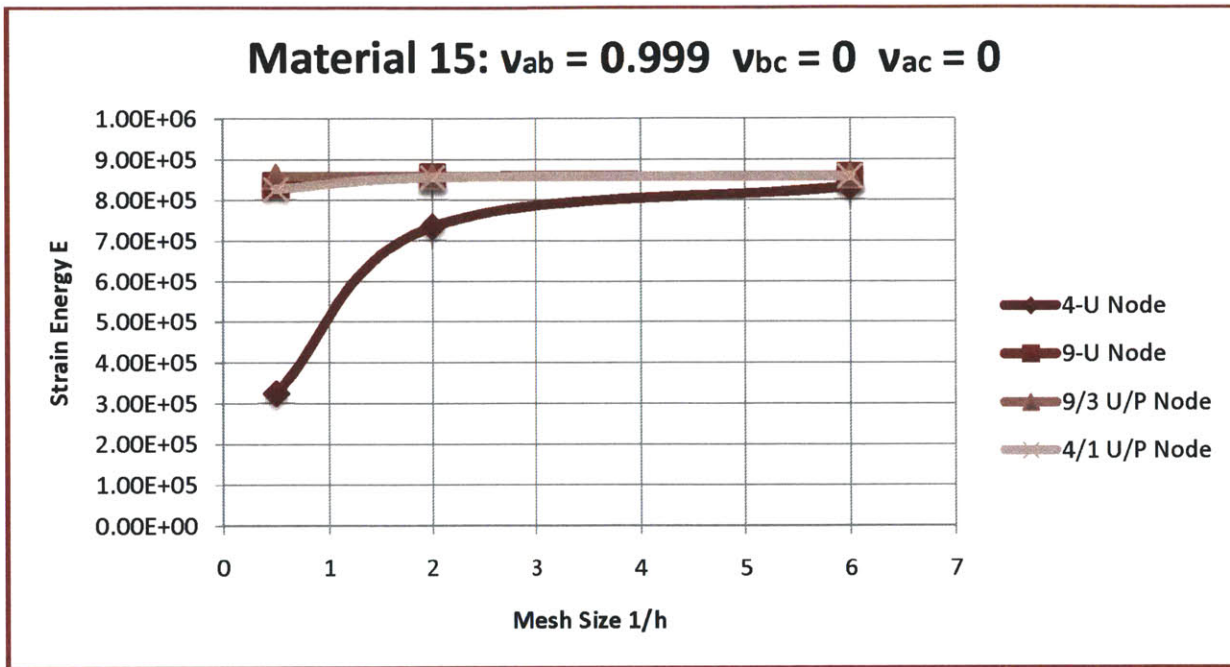
Figure 42: Material 15: vab = 0.999 vbc = 0 vac = 0
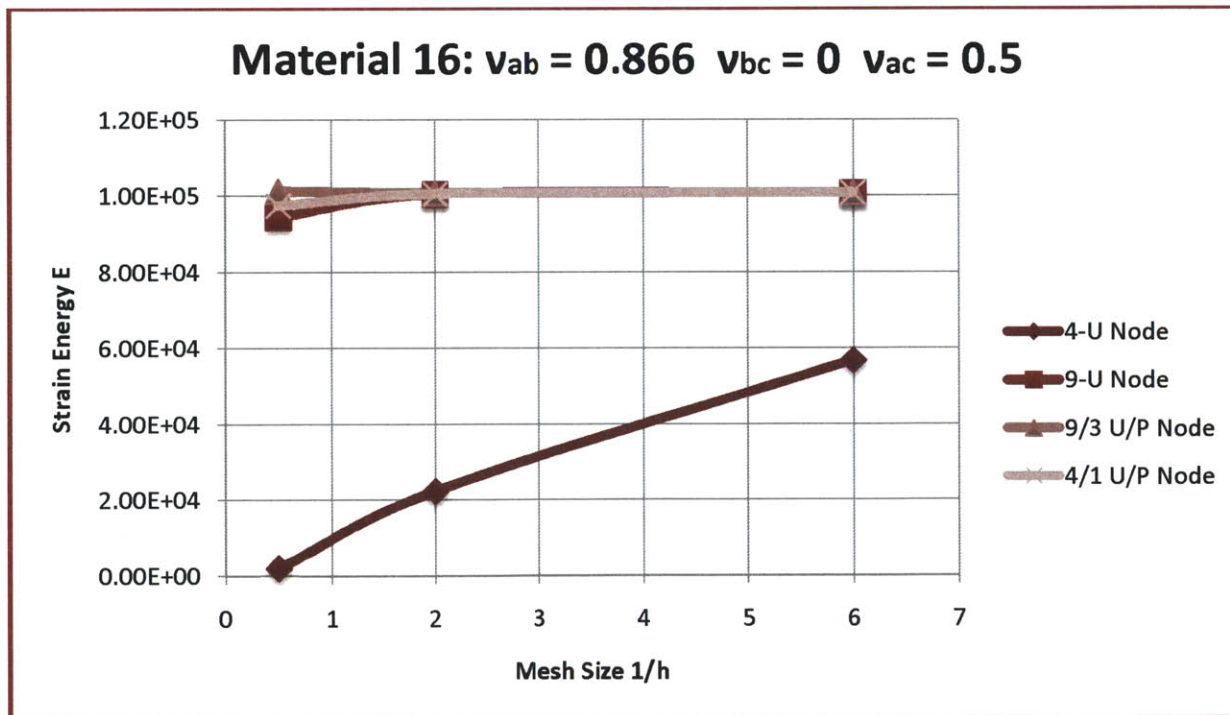
Figure 43: Material 16: vab = 0.866 vbc = 0 vac = 0.5

72
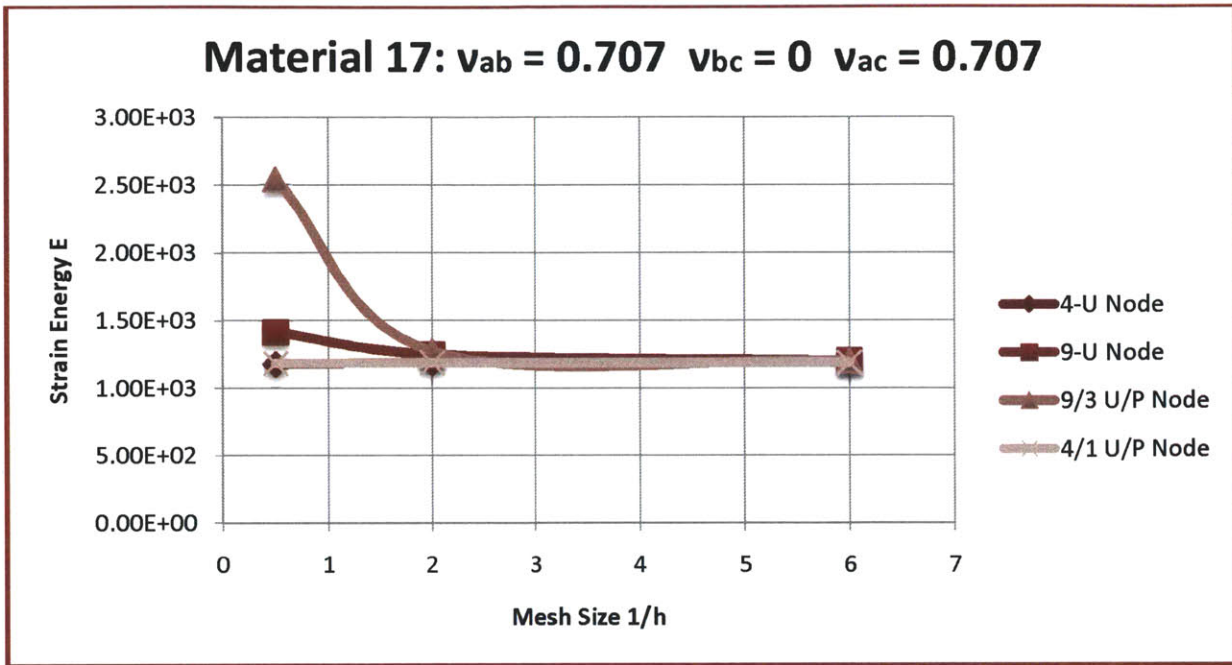
Figure 44: Material 17: vab = 0.707 vbc = 0 vac = 0.707
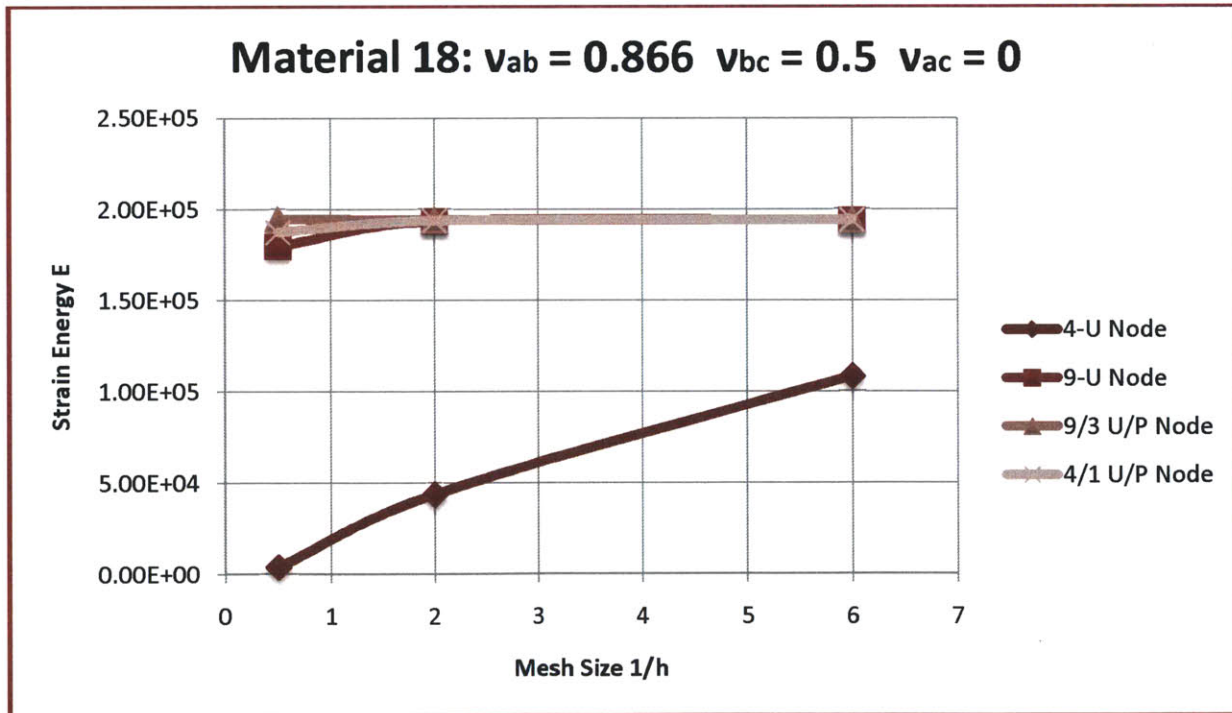
Figure 45: Material 18: vab = 0.866 vbc = 0.5 vac = 0
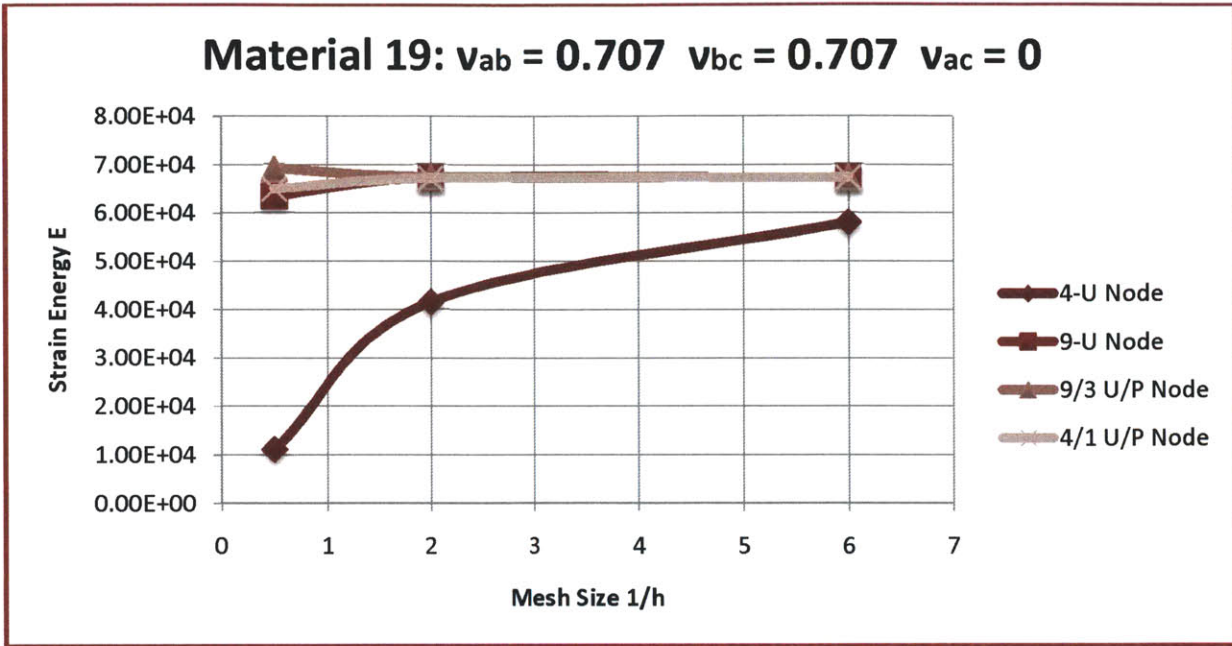
Figure 46: Material 19: vab = 0.707 vbc = 0.707 vac = 0

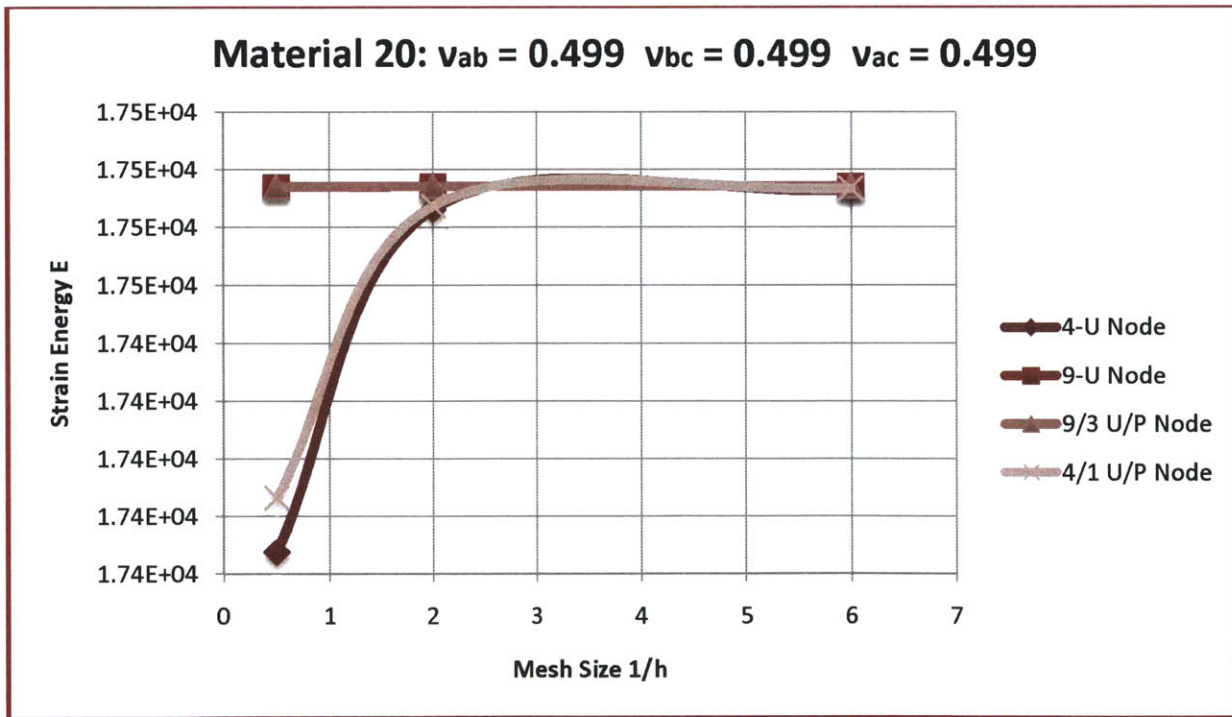**Figure 47: Material 20: vab = 0.499 vbc = 0.499 vac = 0.499**

CONCLUSION

The following was a finite element analysis comparison of the strain energies used for different mesh sizes and for finite elements modeling the loading of a nearly incompressible orthotropic solid sphere. The results are tabulated above. It is shown as predicted, that for all elements used, strain energy converges monotonically with a progressive finer mesh that satisfies the conditions of convergence specified above.

From each of the 20 trials above, it can be seen that the 9 U/P elements had the best convergence rate for nearly incompressible conditions. This means that 9 U/P are just as useful in orthotropic situations as in isotropic situations. Condition 20 performs an isotropic near incompressibility analysis. Just as with isotropic behavior, nearly incompressible conditions arises when the bulk modulus approaches an extremely large value. The definition of the bulk modulus is the same as before but is altered due to each normal strain term now becoming a function of three independent Poisson ratios instead of one. As can be shown in the 3D and axisymmetric models used, the spheres exterior has not changed its surface area due to confined incompressibility.

For the cases involving compressible situations (Material 1 for example), the U/P elements performed competitively to standard 9 node displacement based elements. It is noted though that U/P elements have more degrees of freedom than 9-U Node elements and since they perform competitively, they should not be used in such cases.

Meshes of effective stress show that 4-Node elements have large stress jumps for coarse mesh distributions (1/h = 0.5) and for nearly incompressible situations, these elements behave inadequately. As from before, there is a tradeoff between 4-U Node and 9-U Node elements between computation expense and convergence. It takes longer for 4-U Node elements to converge but the smaller array of D.O.F's used allows quick calculations. Ideally for

75

compressible orthotropic situations, the choice between the two relies with engineering judgment. The same can be said with 4/1 and 9/3 U/P elements depending on whether efficiency or speed should be used respectively. It is the author's opinion that 4 node elements should be used first followed by 9 node elements for comparison.

In conclusion, the assumptions of the relations of these three elements regarding convergence rate and effectiveness for linear isotropic nearly incompressible situations are identical to orthotropic conditions. The only difference is that instead of v = 0.499, the restriction is a function of six variables $f(E_A, E_B, E_C, V_{AB}, V_{BC}, V_{AC})$ that are bounded by restrictions to make the constitutive relation invertible and positive definite. Under these conditions, it is shown that any of the three Poisson ratios may reach values larger than 0.5, the restriction set in isotropic analysis.

REFERENCES

Adina. Theory and Modeling Guide Vol I: Adina. Watertown, M.A.: Adina R&D, Inc., 1999. Print.

Bathe, Klaus. Finite element procedures . Englewood Cliffs, N.J.: Prentice Hall, 1996. Print.

Bauchau, Olivier Andre, and J. I. Craig. Structural analysis with applications to aerospace structures. Dordrecht : Springer, 2009. Print.

Beer, Ferdinand P. Mechanics of Materials. New York, N.Y.: McGraw-Hill, 2006. Print.

Breyer, Donald E.. Design of wood structures--ASD/LRFD . 6th ed. New York: McGraw-Hill, 2007. Print.

Bucalem, Miguel Luiz, and Klaus Bathe. The mechanics of solids and structures hierarchical modeling and the finite element solution. Berlin: Springer, 2011. Print.

Coduto, Donald P.. Geotechnical Engineering Principles and Practices. Upper Saddle River, N.J.: Prentice Hall, 1999. Print.

Cook, Robert Davis. Concepts and applications of finite element analysis. 4th ed. New York, NY: Wiley, 2001. Print.

Kim, Hong. "Nonlinear Analysis of Incompressible Soil Foundation for Gravity Arctic Structures." BP Pipelines 1.1 (1993): 12. Print.

Larson, Holster . Calculus: a multivariable. S.l.: Houghton Mifflin Co, 1999. Print.

Lempriere, B.M.. "Poisson's Ratio in Orthotropic Materials." AIAA 6.11 (1968): 2226. Print.

Ting, T., and T. Chen. "Poisson's Ratio for Anisotropic Elastic Materials can have no bounds." Division of Mechanics and Computation, Stanford University 1.1 (2004): 74-82. Print.

APPENDIX A: PRINCIPLE OF VIRTUAL DISPLACEMENTS DERIVATION

Begin with the differential Formulation of a Solid 3D body. Multiply by a virtual displacement field $\bar{U}_i$. If the following value is always equivalent to zero, then the integral is also equal to 0.

$$\tau_{ij,j} + f_i^B = 0 \qquad \left(\tau_{ij,j} + f_i^B\right)\bar{U}_i = 0 \qquad \int_V \left(\tau_{ij,j} + f_i^B\right)\bar{U}_i\, dV = 0$$

Using the product rule and the divergence theorem from vector calculus

$$\left(\tau_{ij}\bar{U}_i\right)_{,j} = \tau_{ij,j}\bar{U}_i + \tau_{ij}\bar{U}_{i,j}$$

$$\int_V \left[\left(\tau_{ij}\bar{U}_i\right)_{,j} - \tau_{ij}\bar{U}_{i,j} + f_i^B\bar{U}_i\right] dV = 0 \qquad \int_V \left(\tau_{ij}\bar{U}_i\right)_{,j} dV = \int_{S_f} \left(\tau_{ij}\bar{U}_i\right)n_j\, dS_f$$

$$\int_V \left(-\tau_{ij}\bar{U}_{i,j} + f_i^B\bar{U}_i\right)dV + \int_{S_f} \left(\tau_{ij}\bar{U}_i\right)n_j\, dS_f = 0$$

Recognize that the normal product is just the quantities on the surface S$_f$, combine equations

$$\left(\tau_{ij}\bar{U}_i\right)n_j = f_i^{S_f}\bar{U}_i^{S_f} \qquad \int_V \left(-\tau_{ij}\bar{U}_{i,j} + f_i^B\bar{U}_i\right)dV + \int_{S_f} f_i^{S_f}\bar{U}_i^{S_f}\, dS_f = 0$$

Symmetry of the stress tensor is equal to

$$\tau_{ij}\bar{U}_{i,j} = \tau_{ij}\left[\tfrac{1}{2}\left(\bar{U}_{i,j} + \bar{U}_{j,i}\right)\right] = \tau_{ij}\bar{\varepsilon}_{ij} \quad \text{(Linear Theory)}$$

Thus the variational formulation is obtained

$$\int_V \tau_{ij}\bar{\varepsilon}_{ij}\, dV = \int_V f_i^B\bar{U}_i\, dV + \int_{S_f} f_i^{S_f}\bar{U}_i^{S_f}\, dS_f$$

APPENDIX B: UV SPACE TRANSPORTATION DERIVATION

1) We wish to prove the following:

$$\iint_S f(x,y)dxdy = \mp \iint_\Sigma f[x(r,s),y(r,s)]\frac{\partial(x,y)}{\partial(r,s)}drds$$

$$\frac{\partial(x,y)}{\partial(r,s)} = \begin{vmatrix} \dfrac{\partial x}{\partial r} & \dfrac{\partial x}{\partial s} \\ \dfrac{\partial y}{\partial r} & \dfrac{\partial y}{\partial s} \end{vmatrix} = \left|\left(\frac{\partial x}{\partial r}\frac{\partial y}{\partial s} - \frac{\partial y}{\partial r}\frac{\partial x}{\partial s}\right)\right| = |\det (J)|$$

2) The definition of Green's Theorem states that the following two equations are equivalent if F is continuous over the given boundary.

$$F(x,y) = \int_{x_0}^{x} f(t,y)dt \quad , \quad \frac{\partial F}{\partial x} = f(x,y) \quad , \quad \iint_\Omega f(x,y)dxdy = \iint_\Omega \frac{\partial F}{\partial x}dxdy = \oint_{C_1} Fdy$$

3) To transform the above integral into r,s space we create the vector **u** which shall represent the parametric curve C_2 in the r,s space for a $\leq$ t $\leq$ b. Then the vector **x** is a parametric representation for C_1.

$$\mathbf{u}(t) = \langle r(t) \quad s(t)\rangle$$

$$\mathbf{x}(t) = \langle x(t) \quad y(t)\rangle = \langle x(r(t),s(t)) \quad y(r(t),s(t))\rangle$$

$$\oint_{C_1} F(x,y)dy = \int_a^b F\big(x(r(t),s(t)),y(r(t),s(t))\big)\frac{dy}{dt}dt$$

4) Apply the chain rule on y=y(r,s) to yield the following.

$$\frac{dy}{dt} = \frac{\partial y}{\partial r}r'(t) + \frac{\partial y}{\partial s}s'(t)$$

79

5) Simplify and substitute.

$$\bar{F} = \bar{F}(r,s) = F\left(x(r(t),s(t)), y(r(t),s(t))\right) = F(x(r,s), y(r,s))$$

$$\oint_{C_1} F(x,y)dy = \int_a^b \bar{F}(r(t),s(t))\left[\frac{\partial y}{\partial r}r'(t) + \frac{\partial y}{\partial s}s'(t)\right]dt = \int_a^b \left[\bar{F}\frac{\partial y}{\partial r}r'(t) + \bar{F}\frac{\partial y}{\partial s}s'(t)\right]dt$$

$$\oint_{C_1} F(x,y)dy = \mp \oint_{C_1} \left(\bar{F}\frac{\partial y}{\partial r}dr + \bar{F}\frac{\partial y}{\partial s}ds\right)$$

$$\oint_{C_2} (Pdr + Qds) = \iint_{\Sigma} \left(\frac{\partial Q}{\partial r} - \frac{\partial P}{\partial s}\right)drds$$

$$\frac{\partial Q}{\partial r} = \frac{\partial \bar{F}}{\partial r}\frac{\partial x}{\partial s} + \bar{F}\frac{\partial^2 x}{\partial r\partial s}$$

$$\frac{\partial P}{\partial s} = \frac{\partial \bar{F}}{\partial r}\frac{\partial x}{\partial s} + \bar{F}\frac{\partial^2 x}{\partial r\partial s}$$

$$\oint_{C_1} Fdy = \mp \iint_{\Sigma} \left(\frac{\partial \bar{F}}{\partial r}\frac{\partial y}{\partial s} + \bar{F}\frac{\partial^2 y}{\partial r\partial s} - \frac{\partial \bar{F}}{\partial s}\frac{\partial y}{\partial r} - \bar{F}\frac{\partial^2 y}{\partial s\partial r}\right)dudv = \mp \iint_{\Sigma} \left(\frac{\partial \bar{F}}{\partial r}\frac{\partial y}{\partial s} - \frac{\partial \bar{F}}{\partial s}\frac{\partial y}{\partial r}\right)dudv$$

$$\frac{\partial \bar{F}}{\partial r} = \frac{\partial \bar{F}}{\partial x}\frac{\partial x}{\partial r} + \frac{\partial \bar{F}}{\partial y}\frac{\partial y}{\partial r} \qquad \frac{\partial \bar{F}}{\partial s} = \frac{\partial \bar{F}}{\partial x}\frac{\partial x}{\partial s} + \frac{\partial \bar{F}}{\partial y}\frac{\partial y}{\partial s}$$

$$\oint_{C_1} Fdy = \mp \iint_{\Sigma} \left[\left(\frac{\partial \bar{F}}{\partial x}\frac{\partial x}{\partial r} + \frac{\partial \bar{F}}{\partial y}\frac{\partial y}{\partial r}\right)\frac{\partial \bar{y}}{\partial s} - \left(\frac{\partial \bar{F}}{\partial x}\frac{\partial x}{\partial s} + \bar{F}\frac{\partial \bar{F}}{\partial y}\frac{\partial y}{\partial s}\right)\frac{\partial y}{\partial r}\right]drds$$

$$\oint_{C_1} Fdy = \iint_{\Sigma} \frac{\partial \bar{F}}{\partial x}\left(\frac{\partial \bar{x}}{\partial r}\frac{\partial y}{\partial s} + \bar{F}\frac{\partial x\partial y}{\partial s\partial r}\right)drds$$

$$\oint_{C_1} Fdy = \mp \iint_{\Sigma} f(x(r,s), y(r,s))\frac{\partial(x,y)}{\partial(r,s)}drds$$

$$\iint_{\Omega} f(x,y)dxdy = \iint_{\Omega} \frac{\partial F}{\partial x}dxdy = \oint_{C_1} Fdy = \iint_{\Sigma} f(x(r,s), y(r,s))\frac{\partial(x,y)}{\partial(r,s)}drds$$